Final Technical Report

for

Sulfur Oxidation and Contrail Precursor Chemistry

NASA Grant Number
NAG3-2674

Grant Duration
October 15, 2001 through December 19, 2004

Kenneth DeWitt
Principal Investigator

Soon M. Hwang
Research Associate

Department of Mechanical, Industrial and Manufacturing Engineering
University of Toledo
Toledo, Ohio 43606

March 8, 2005

An Abstract of

DETERMINATION OF THE RATE COEFFICENTS OF $SO_2 + O + M = SO_3 + M$ REACTION

John Thomas Winter

Submitted in partial fulfillment of the requirements for the Master of Science in Mechanical Engineering Degree

The University of Toledo
August 2001

Sulfuric acid (H_2SO_4), formed in commercial aircraft operations via Fuel-S → SO_2 → SO_3 → H_2SO_4, plays an important role in affecting the global climate change through atmospheric chemical reactions and radiative forcing. Measurement of the sulfur oxidation rates is critical to the understanding of the contrail formation. The principle reaction pathway is

$$SO_2 + O + M \rightarrow SO_3 + M \qquad \text{(R21)}.$$

Although there are many measurements for the rates of this reaction, it has never been measured in the temperature and pressure regime available to aircraft operation. In this investigation, a series of experiments were performed behind the reflected shock waves in a shock tube. OH radicals were produced in lean, shock heated $SO_2/H_2/O_2/Ar$ mixtures. The reaction progress was followed using OH absorption spectroscopy at 310 nm. The data were analyzed with the aid of computer modeling/simulation.

The mean value of the rate coefficients of R21 determined is

$$k_{21,0}/[M] = 3.9 \times 10^{15}\ \text{cm}^6\ \text{mol}^{-2}\ \text{sec}^{-1}$$

at $T = 960$ - 1150 K and $\rho = 16$ - 30 μmol cm^{-3} with uncertainty limits of ±30%.

A non-Arrhenius fit to our data together with all existing data gives

$$k_{21,0}/[\mathrm{M}] = 1.3 \times 10^{24}\, T^{-2.5} \exp(-2350\ \mathrm{K}/T)\ \mathrm{cm}^6\ \mathrm{mol}^{-2}\ \mathrm{s}^{-1}$$

at $T = 300$ - 2500 K with the same uncertainty limits given above. The calculated conversion of S(IV) (SO_2) to S(VI) ($SO_3 + H_2SO_4$) was about 2% in our experimental conditions.

Acknowledgements

I wish to express my deepest appreciation to Dr. Kenneth J. De Witt, my thesis adviser, for his invaluable advice, encouragement, and support throughout my study at the University of Toledo. It has been a pleasure studying under his guidance. These wishes must also be extended to Dr. Soon Muk Hwang for his advice and help during the thesis experiments and data analysis. He made invaluable contributions to this work. Dr. Martin J. Rabinowitz of the NASA Glenn Research Center at Lewis Field deserves special thanks for providing me with this opportunity to work and for his generous advice and help throughout this thesis research. The financial support from the NASA Glenn Research Center at Lewis Field and the Department of Mechanical Engineering at the University of Toledo is gratefully acknowledged. All the experiments and computations in this work were performed at the NASA Glenn Research Center at Lewis Field in Cleveland, Ohio.

Heartfelt thanks to my parents, Scott and Carol, for their unconditional love and support over the past 25 years. Thanks to my brother and his wife, Jeremy and Cindy, as they graciously opened their home to me. To my fiancé, Katie, for her support and sharing all difficulties with me throughout this study.

Table of Contents

List of Tables

List of Figures

Introduction

Aircraft aerosol emissions (condensation trails; contrails) are often the most visible evidence of aircraft traffic.[1] Contrails are formed whenever the requisite conditions of either ice or water supersaturation exists within aircraft exhaust plumes. The role of contrails in the formation of cirrus clouds has been debated for years.[2, 3] Natural cirrus clouds and contrail induced cirrus clouds affect the global climate via alterations of atmospheric photochemistry and radiative forcing.[4, 5] Studies[6] showed that the absence of aircraft induced cirrus clouds during the three-day grounding of all commercial aircraft in the United States following the terrorist attacks on 11 September 2001 increased the average air temperature difference between the daytime maximum and night-time minimum temperatures. I.e. cirrus clouds affect the global climate by altering the Earth's radiative energy budget through both scattering incoming sun light and reflecting radiation from the Earth's surface.[4, 5] Scattering sunlight reduces the amount of heat reaching the Earth's surface resulting in a lower daytime maximum temperature. Reflecting radiation from the Earth's surface increases the heat retention at night resulting in a higher night-time minimum temperature.

Measurements of the composition and particle size distribution within contrails[7-9] indicate that, in addition to exhaust soot and water vapor, sulfates and sulfuric acid formed

by the oxidation of fuel sulfur are critical components of exhaust aerosols. Sulfuric acid and sulfates in aircraft exhaust plume facilitate heterogeneous processing for nitrogen oxide and halogen reservoir gases for ozone depletion and enhance nucleation of aerosol particles to form persistent contrails and cirrus clouds. Sulfuric acid was assumed to form liquid volatile particles by binary homogeneous nucleation,[10] to interact with soot,[11] and to affect contrail formation.[12] Two possible mechanisms for the formation of contrails have been considered: (1) in the engine exhaust plume, sulfuric acid (H_2SO_4) is formed via homogeneous conversion of Fuel-S $\rightarrow$ SO_2 $\rightarrow$ SO_3 $\rightarrow$ H_2SO_4 followed by aerosol particle inception via binary nucleation of H_2SO_4/H_2O; and (2) heterogeneous condensation of H_2SO_4/H_2O on soot particles or ions. Sulfuric acid enables contrail formation at higher temperatures than without it by lowering the saturation vapor pressure of H_2SO_4/H_2O.

Numerous flight experiments have measured the particle and contrail formation properties in aircraft exhaust plumes for different fuel sulfur content (FSC, 2 - 5500 ppm), flight conditions, and aircraft (ATTAS, A340, B707, B737, DC8, DC10) in the years from 1994 to 1999 (see Table I[54]). In October 1994, particle measurements in the exhaust plume of a Concorde supersonic aircraft flight revealed larger number concentrations of small particles within aircraft exhaust plumes than expected.[13] Also a very large conversion fraction of fuel sulfur to sulfuric acid, ϵ, was derived, larger than 12%, possibly exceeding 45%. This large sulfur conversion fraction reported by Fahey et al.[13] was explained by invoking the assumption that a large fraction of the Fuel-S has already been converted to S(VI) ($SO_3 + H_2SO_4$) before leaving the engine exit.[14-16]

The only direct measurements of sulfuric acid in the exhaust plume of cruising aircraft are those obtained from the Advanced Technology Testing Aircraft System

(ATTAS) and B737 aircraft. The measurement method applied was the Volatile Aerosol Component Analyzer (VACA): Chemi Ionization Mass Spectrometry (CIMS). Measurements show a conversion of Fuel-S to H_2SO_4, S(VI), around 0.34 - 4.5%.[17] Models show OH contributed only 1 - 2% toward the oxidation of SO_2, S(IV) in the plume.[18] The measurements behind the ATTAS reveal a conversion of Fuel-S to sulfuric acid, $\epsilon < 0.34\%$,[17] consistent with direct measurements at ground ($\epsilon = 1.2\%$, at FSC of 212 ppm),[19] and also in accordance with the early result ($\epsilon > 0.4\%$) measured at ground by Frenzel and Arnold 1994.[20] For the B737, ϵ is measured to be $3.3 \pm 1.8\%$ for the rather low FSC of 56 ppm.[21] In Table I, the listed apparent ϵ values (denoted by ϵ^*) are derived from volatile particle volume measurements in the young exhaust plume for various FSC values. For low FSC values some of the results imply $\epsilon^* > 50\%$. The low-sulfur aerosol data measured behind the ATTAS would imply even larger ϵ^* fractions than derived elsewhere. The strong increase in the aerosol derived ϵ^* for small FSC values indicates that condensable gases other than sulfuric acid contribute to the formation of volatile particles in the young exhaust plume.

Table I. Flight Experimental Measurements [a]

FSC[b] (ppm)	Aircraft	Engine	Altitude (km)	Temp. (°C)	Pressure (Torr)	RH (water) (%)	V ($m\ s^{-1}$)	Plume age (sec)	ϵ, (%)	$Mass_{soot}$ ($g\ kg^{-1}$)	PEI_{soot} ($10^{15}\ kg^{-1}$)	PEI_{total} ($10^{15}\ kg^{-1}$)	Contrail Seen	Reference
2	ATTAS	VFW 614	9.1	-50	227	34	115	> 0.3	...	...	...	...	yes	9
2.6	B737	CFM56-3B1	7.9	-30	270	55 - 65	167	0.2 - 0.6	>17 ± 6[c]	0.011 ± 0.005	0.35	60	no	22
2.6	ATTAS	Mk501	7.9	-38	269	35 - 40	153	0.5 - 7	>20 - 80[c]	0.1 ± 0.02	1.8	100	no	22
22	ATTAS	Mk501	7.9	-42	270	50 - 65	160	>0.5	0.34 < ϵ < 4.5[c]	...	...	...	no	17, 23
56	B737	CFM56-3B1	7.9	-30	270	55 - 65	167	0.2 - 0.6	>2.4 ± 0.8[c]	0.011 ± 0.005	0.35	90	no	22
56	B737	CFM56-3B1	5.8	-14	368	75 - 85	141	>0.15	3.3 ± 1.8	...	...	...	no	21
118	ATTAS	Mk501	9.8	-52	206	35 - 50	177	>0.5	2.3[c]	0.1 ± 0.02	1.8	150	no	22
120	B707	JT3D-3B	9.5	-42	216	20	187	0.4 - 0.7	(0.4 - 21)[c]	0.5 ± 0.1	1.7	6	no	23
170	ATTAS	Mk501	9.5	-55	215	50	163	20	(0.4 - 1.8)[c]	...	...	8	yes	24
230	Concorde	Olympus 593	16.1	-51	75	...	255	780 - 3360	>12,[c] >46[c]	...	43 - 87	17 - 650	yes	13
250	ATTAS	VFW 614	9.1	-50	227	44	115	> 0.3	...	...	...	...	yes	9
380	A340	CFM56-5C4	9.6	-42	211	20	194	0.5 - 0.8	(1.6 - 22)[c]	0.01 ± 0.003	0.18	48 (32 - 100)	no	23
480	A340	CFM 56-2C1	10.7	-51	179	29	200	100	...	...	1.6	19 - 23	yes	25
2700	ATTAS	Mk501	7.9	-42	270	50 - 65	160	>0.5	0.34 < ϵ < 1.8[c]	...	...	...	no	17, 23
5500	ATTAS	Mk501	9.5	-55	215	50	163	20	(0.4 - 1.8)[c]	...	...	10	yes	24

[a] The table is ordered by fuel sulfur content (FSC); ambient values used for the temperature and pressure, relative humidity of liquid saturation (RH), ϵ = conversion mole fraction of fuel sulfur to sulfuric acid, $Mass_{soot}$ = soot mass, PEIsoot and PEItotal = particle number emission indices of nonvolatile or "soot" particles and total (including volatile) particles per unit mass of fuel burned. Values in parentheses denote the possible range of results from the experiments.

[b] The fuel analyses (~20 sample) imply a combustion heat Q = 43.21 ± 0.06 MJ kg-1, and a hydrogen mass fraction of 13.71 ± 0.1% (EIH2O = 1.225 ± 0.01; EICO2 = 3.16 ± 0.005).

[c] Calculated from particulate volume and presuming that the particles are exclusively composed of sulfuric acid and water, denoted by epsilon star in the text.

In summary, the conversion fraction ϵ of Fuel-S to sulfuric acid is measured in the range 0.34 to 4.5% for an older (Mk501) and 3.3 ± 1.8% for a modern engine (CFM56-3B1). For low FSC, ϵ is considerably smaller than what is implied by the volume of volatile particles in the exhaust ($\epsilon < \epsilon^*$).

In the homogeneous gas phase, sulfuric acid is believed to be formed via the following reactions:

$$\text{Fuel-S} \rightarrow \quad \rightarrow \ SO_2$$

$$SO_2 + O + M \rightarrow \ SO_3 + M \qquad \text{(R21)}$$

$$SO_2 + OH\ (+M) \rightarrow \ HOSO_2\ (+M) \qquad \text{(R30)}$$

$$HOSO_2 + O_2 \rightarrow \ SO_3 + HO_2 \qquad \text{(R40)}$$

$$SO_3 + nH_2O \rightarrow \ H_2SO_4 + (n\text{-}1)H_2O,\ n = 1\text{-}4 \qquad \text{(R36)}$$

All Fuel-S is oxidized inside the combustor to SO_2 (S(IV)) and a small amount of SO_2 is believed to undergo further oxidation to SO_3 (S(VI)). Kinetic calculations predict that less than 4% of the sulfur is in S(VI) and OH contributed 1 - 2% toward the oxidation of SO_2 in the plume[18] while, as described above, measurements show 0.34 - 4.5% conversion.[17] The principal reaction pathway hinges primarily upon the rate coefficient of Reaction 21.

In the following, a brief review of the previous experiments for the R21 is given. Nettleton and Stirling[26] explored R21 at 2150 K. In their flow reactor experiments, a coaxial nozzle was used to introduce a mixture of fuel (oxygen and sulfur dioxide diluted with an appropriate amount of nitrogen) into an alumina tube wound with a molybdenum heater. The reaction products were sampled isokinetically through a 1-mm-bore alumina

tube. The sampling tube was heated electrically to avoid condensation of sulfur dioxide and the assembly was enclosed in a water-cooled jacket. The rates of SO_3 formation and SO_2 depletion were measured using the electrical conductivity of a solution in conjunction with iodine titrations by Laxton's methods. Using nitrogen as a collision partner (M), they determined the value of $k_{21,0}/[M] = 2 \times 10^{15}$ cm^6 mol^{-2} sec^{-1} at 2150 K.

Westenberg and deHaas[27] studied R21 over the temperature range of 248 - 415 K using a fast flow reactor system. They used M = He. O-atom generation was done by microwave discharge of trace amounts of O_2 (<0.2%) carried in He. Pseudo-first-order decays of O were monitored with an ESR cavity at a fixed position downstream of the heated or cooled reactor. The reaction time was varied by means of a movable injector through which excess flows of SO_2 were introduced. Metering of SO_2 was done for each run by switching the flow from the injector into a calibrated volume and timing the pressure rise on a Kel-F oil manometer. The reactor walls were both cleaned and coated with boric acid. The recommended rate coefficient was $k_{21,0}/[M] = 3.9 \times 10^{16} \exp[-(1400 \pm 50)\ K/T]$ cm^6 mol^{-2} sec^{-1}.

Astholz et al.[28] studied R –21 ($SO_3 + M \rightarrow SO_2 + O + M$) over the temperature range of 1700 - 2500 K using a shock tube technique. The experiments were performed behind the incident or the reflected shock waves in a shock tube with inner walls made of aluminium and having a 10 cm inner diameter. Decomposition of SO_3 was followed by monitoring SO_2 via Ultraviolet absorption. The possible removal of SO_2 by adsorption on the shock tube was regarded as unimportant. Ar was used for M. The recommended rate coefficient (R –21) expression was $k_{-21,0} = 3.16 \times 10^{15} \exp(-31874\ K/T)$ cm^3 mol^{-1} sec^{-1}.

Atkinson and Pitts[29] investigated R21 over the temperature range of 298 - 440 K. A flash photolysis-NO_2 chemiluminescence technique was employed. $O(^3P)$ atoms were produced by the pulsed vacuum ultraviolet photodissociation of SO_2 (0 - 2.35 Torr) and/or NO (0.020 - 0.093 Torr) at wavelengths longer than the CaF_2 cutoff ($\geq$1250 Å). $O(^3P)$ atom concentrations were monitored as a function of time after the flash by NO_2 chemiluminescence formed via $O + NO + M \rightarrow NO_2^* + M$ and $NO_2^* \rightarrow NO_2 + h\nu$. Signals were obtained by photon counting in conjunction with multichannel scaling. Decays of the NO_2 chemiluminescence, hence of $O(^3P)$ atom concentration were accumulated from 65-1040 flashes depending on the signal strengths. Ar, N_2 and SO_2 were used as collision partners. The recommended rate coefficients taken over the temperature range of 298 - 440 K was $k_{21,0}/[Ar] = 1.12 \times 10^{16} \exp(-1009\ K/T)\ cm^6\ mol^{-2}\ sec^{-1}$. The recommended rate coefficients (in the unit of $cm^6\ mol^{-2}\ sec^{-1}$) at $T = 298.15$ K were $k_{21,0}/[Ar] = 3.9 \times 10^{14}$, $k_{21,0}/[N_2] = 5.0 \times 10^{14}$, $k_{21,0}/[SO_2] = 3.5 \times 10^{15}$, so that the corresponding collision efficiencies are $\epsilon_{SO2}: \epsilon_{O2}: \epsilon_{Ar}: = 9.0 : 1.3 : 1.0$. Any heterogeneous reactions were not considered.

Merryman and Levy[30] studied R21 at 1685 K using a quartz tube burner. The quartz tube burner allowed them to establish stable methane-H_2S flames within desired fuel-air ratios. Two inlets were provided above the flame (first stage) for adding air to complete the combustion process (second stage). SO_3 was then sampled at various positions downstream of the secondary air. The reaction chamber was externally heated (Chromel-A wiring) to control second stage temperatures. Gas samples were removed at various locations above the flame via a quartz sampling probe. SO_3 was removed from the gas as H_2SO_4 using a Goksoyr-Ross type (micro) collection apparatus and was determined

colorimetrically by the barium Chloranilate procedure. CO, CO_2, O_2, and SO_2 were also measured, mainly for purposes of confirming and comparing postflame combustion conditions and sulfur oxide levels with calculated cold gas compositions. The determined rate coefficient in a methane-H_2S flame was $k_{21,0}/[M]= 7.4 \times 10^{14}$ cm^6 mol^{-2} sec^{-1}. It was observed that increasing the flame pressure increases SO_3 formation.

Smith et al.[31] evaluated R21 from the kinetic scheme along with the measured species concentrations profiles over the temperature and pressure range of 1435 - 1850 K and 200 Torr, respectively, by means of a flame and a nozzle-beam-skimmer mass-spectrometer sampling system. The reaction of R21 was studied in a $CO/O_2/Ar$ flame doped with small amounts of SO_2. The flame was stabilized at 0.26 atm (200 Torr) on an uncooled stainless-steel flameholder. Mass spectrometric measurements of species concentration profiles (CO, O_2, CO_2, O and SO_3) using a nozzle-beam-skimmer sampling system. After their sampling and detection system was calibrated and corrected for the pressure diffusion, skimmer or 'mach disk' interference, background scattering, and 'mach number' or 'speed-ratio' focusing, they then obtained the net formation rate for SO_3 as a function of distance from the burner (a function of temperature). They recommended the rate coefficient expression of $k_{21,0}/[Ar] = 4.4 \times 10^{14} \exp(3163\ K/T)$ cm^6 mol^{-2} sec^{-1}.

The rate coefficients of the spin-forbidden title reaction, $SO_2(^1A_1) + O(^3P) + M \rightarrow SO_3(^1A_2) + M$ show some peculiar behavior; the $k_{21,0}/[M]$ values increase with temperature at $T < 450$ K, reach a maximum value and then decrease rapidly as temperature increases further. In 1978 the rate coefficients of this reaction were calculated by Troe[32] using Rice, Ramsperger and Kassel (RRK) theory. The calculated rate coefficients were fitted into a

non-Arrhenius expression, $k_{21,0}/[Ar] = 10^{16.6} (T/1000\ K)^{-4} \exp(-2667\ K/T)\ cm^6\ mol^{-2}\ sec^{-1}$ at $T = 300$- 2500 K.

Although R21 has been investigated by many authors, the rates of this reaction have never been measured in the temperature and pressure regime available to aircraft operation (900 - 1200 K, 0.13 - 0.30 atm). Figure 8 illustrates the previous results for R21, showing that a clear consensus does not exist in the high temperature region and the lack of measurements in the temperature region of interest. In this investigation, a series of experiments was performed behind the reflected shock waves to provide the rate data in the temperature regime of aircraft operation. The reaction progress was followed by monitoring OH radicals produced in lean, shock heated $SO_2/H_2/O_2/Ar$ mixtures using OH laser absorption in spectroscopy at 310 nm. The data were analyzed with the aid of computer modeling/simulation. Rate coefficients were derived by matching experimental absorption profiles.

Experimental Section

Shock Tube System

Experiments were performed in a rolled square stainless steel shock tube with an internal cross section of 63.5 mm x 63.5 mm. The length of the driven section was 5.5 m and the driver section was 2.2 m. The driver section was separated from the driven section by an unscored dead-soft-temper aluminum diaphragm (Alufoil Products Co.) and pumped with a Varian SD-91 roughing pump. A Varian zeolite-sieve was used to trap the oil backstreaming from the roughing pump. Pressure in the driver section was always maintained above 500 microns to further reduce the effects of back streaming. The diaphragm was burst with a cross-shaped plunger. Mixtures of He and Ar served as the driver gas. A schematic diagram for the experimental setup is given in Figure 1.

The driven section was routinely pumped to approximately 3×10^{-6} Torr by a Varian SD-700 roughing pump and a Varian V60 Turbopump equipped with a Varian SD-90 fore pump. The combined leak and outgassing rate was about 5×10^{-6} Torr min^{-1}. All shocks were initiated within one minute of filling the driver section with the test gas.

The gas handling system was constructed with high vacuum Varian valves (Model # L6591-301) and seals. The vacuum pressure of the driven section and the gas handling system was measured by three Varian 0531 thermocouple gauges coupled to Varian 801

vacuum readouts and a Varian 525 cold cathode gauge with a Varian 860A vacuum readout. Both the reactant pressures in the mixing tanks and the initial test gas pressures in the shock tube were measured by a Druck Model DPI-260, 200 Torr pressure transducer (accuracy of 0.01 Torr) and a DPI-260, 5000 Torr pressure transducer (accuracy of 1 Torr).

Two 25.4 mm diameter S1-UVA quartz windows were flush mounted on opposite sides of the shock tube inner walls. The shock tube velocities were measured using four flush-mounted 113A21 PCB Piezotronics pressure transducers powered by a PCB 482A05 Piezotronics power supply. The distances between the pressure transducers were 7.62 cm, 30.48 cm, and 15.24 cm downstream from the end wall. The last transducer was positioned 1.27 cm from the end wall.

The pressure transducers triggered 3 Phillips PM6666 programmable timers ($\geq$20 MHz). The incident shock velocities, measured between the pressure transducers, were fitted to a second order polynomial as a function of distance from the first pressure transducer. The shock velocity at the end wall was determined by extrapolation of the fitted polynomial. This velocity was then used to calculate the shock properties behind the reflected shock wave. The procedure automatically accounted for and incorporated for shock wave attenuation. The shock properties were computed by standard methods[33] using NASA thermodynamic data.[34] The computed shock properties were corrected for boundary layer/reflected shock interaction effects using the similar method of Michael and Sutherland.[35-37] It was assumed that full vibrational relaxation was achieved and no chemical reactions occurred at the shock front.

Detection System

The combined OH and SO_2 absorption profiles were measured at 310.032 nm (air), corresponding to the $P_1(5)$ line of the (0,0) band of the OH $A^2\Sigma^+ \leftarrow X^2\Pi$ transition. A Coherent CR-899-21 ring-dye laser running with Kiton Red 620 dye (Exciton Chemical Co.) was pumped by a Coherent Innova 200 argon ion laser. A Coherent 5920 Dye Circulator at pressures between 35 and 42 psi circulated the dye solution (Kiton Red 620 dye dissolved in methanol and ethylene glycol). The temperature of the dye solution was maintained at 5°C by a Neslab CFT-25 Refrigerated Recirculator in order to achieve maximum conversion efficiency. The concentration of the dye solution was controlled so that 90% of the argon ion laser beam was absorbed in the dye jet. The argon ion laser was operated in single line (514.5 nm) and light regulation (7.5 ± 0.038 W) modes. Adjusting the dye laser cavity length actively stabilized the ring-dye laser. An error signal generated by filtering out the amplitude information of a mode locked laser beam in a reference cavity was amplified and used to drive a high frequency piezoelectric mounted folding mirror and a scanning Brewster plate to adjust the cavity length. Single frequency operation out of the CR-899-21 ring-dye laser was achieved by using a three-plate birefringent filter and an intracavity assembly (a thin etalon and a piezoelectric driven thick etalon).

Ultraviolet (UV) output (310.032 nm in air) was generated via intracavity doubling of the fundamental beam using a Coherent Model 7500 frequency doubler ($LiIO_3$ crystal). The wavelength of the primary beam was monitored by a Burleigh WA-10 Wavemeter with a readout precision of ±0.001 nm. The resulting single mode UV beam had a line width of 2 MHz and a typical output power of ~ 5 mW. Laser wavelength was varied

using the electronic controller until maximum absorption within a burner stabilized CH_4/Air flame was reached. At that time the 899 - 21 ring-dye laser was placed in "Lock" mode. Frequency lock was then actively controlled by the laser electronics with no measurable deviation for the time between wavelength locking and shock arrival (approximately 30 seconds). The lasers, optical components, as well as the detection system described next were mounted on a pneumatically stabilized Newport MST series optical table.

For signal detection of OH radicals and SO_2 molecules, a triple beam scheme was employed. The UV beam was first split into two beams using a UV beam splitter (Esco Products, Inc.). The primary beam was directed through the center of the two 25.4 mm diameter S1-UVA quartz windows, 12.7 mm distant from the shock tube end wall. If the expected absorbance for an experiment was small, the beam was reflected back through the shock tube at the same streamwise distance and vertically displaced from the incoming beam and onto a PMT (THORN EMI Model 9924QB photomultiplier tubes), i.e., double pass. For an experiment with larger expected absorbance, the beam was returned to a PMT after being steered around the shock tube, i.e., single pass. The secondary beam was split again into two beams, one passed through a burner-stabilized CH_4/air flame used to locate the center absorption wavelength, λ_o, and the other for the reference signal used for noise reduction. An iris was set in front of the probe signal beam detector both to limit emission from the hot gases within the shock tube and to establish the "Time Zero" from the schlieren peaks produced by shock passage. A customized five-dynode configuration was used for each PMT to guarantee optimum linearity for the light intensity of the UV laser beams. A high-speed buffer/amplifier (National Semiconductor LH0033CG) isolated the

anode from the coaxial signal cable. The overall electronic time constant determined for the entire PMT—buffer—cable system was less than 0.5 μs. Background light reduction was achieved by mounting a narrow band interference filter (Pomfret Research Optics, Inc., Model # 20-3100-1, $\lambda_o \pm \Delta\lambda$ (FWHM) = 310 ± 10 nm) in front of each PMT. Also, during the course of experiments the room lights were turned off. The reference signal, the probe signal, the difference (probe dc – reference ac), and the signal from the last pressure transducer were recorded by a four-channel Nicolet 4094C digital oscilloscope equipped with Nicolet 4570 plug-in units. The pressure signal served as the trigger source for the oscilloscope. Reaction progress was followed using the difference signal. The signal-to-noise ratio was usually better than 70.

Absolute pressure in the shock tube was measured using the voltage signal of the 113A21 PCB Piezotronics pressure transducer, deliberately mounted in line with the windows. The voltage output was then converted to absolute pressure using a calibration curve supplied with the transducer by the manufacturer. The calibration was validated against a dead weight gauge at the NASA Glenn Research Center Calibration Laboratory before use. The initial test gas pressure was added to this pressure. This actual pressure was then used in the temperature correction for the boundary layer effects.

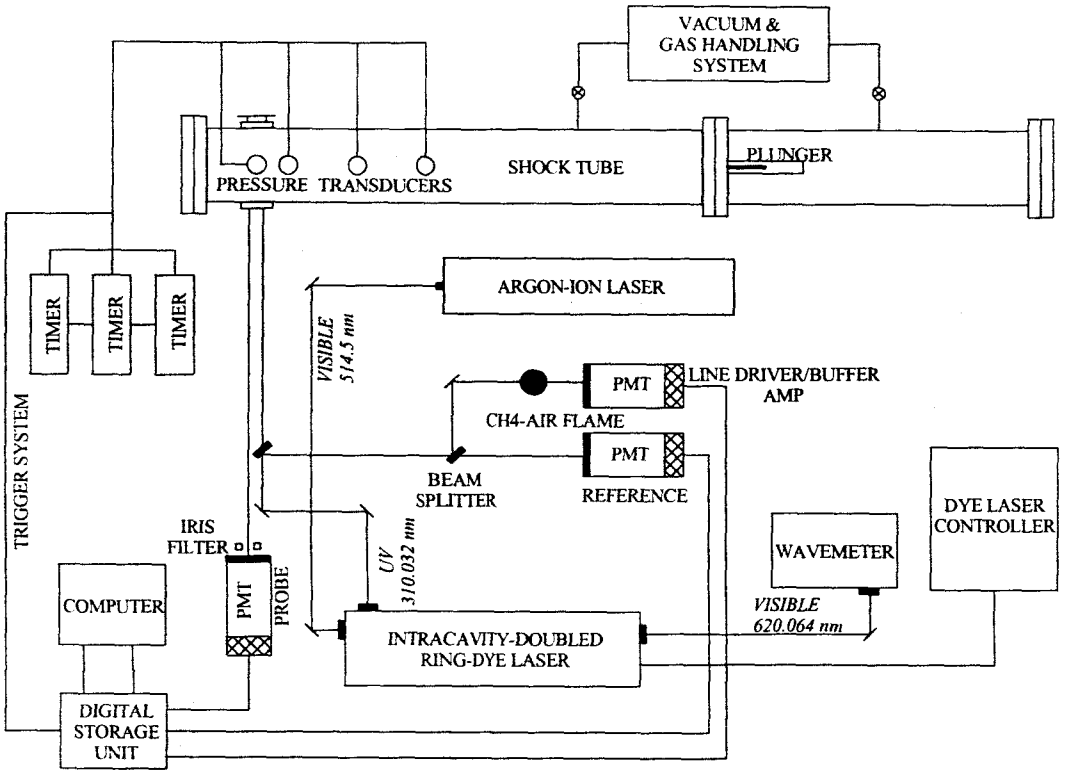

Figure 1: Schematic Diagram of the Experimental Setup

Test Gas Mixture Preparation

All test gas mixtures were prepared manometrically and allowed to stand for at least 48 hours before use. The maximum uncertainty of the species concentrations in the final mixture was less than 0.5% of the nominal mole fraction for each component. The stated purities of the gases were: H_2, 99.9995% (MG Industries, Scientific grade); O_2, 99.998% (MG Industries, Scientific grade); Ar, 99.9999% (MG Industries, Sputtering grade); SO_2 (anhydrous), 99.98 wt.% (MG Industries, Scientific Grade). All gases were used without further purification.

Thermodynamic Data of Relevant Species of $SO_2/H_2/O_2$ System

In computer modeling using a reaction mechanism for practical combustion systems or for extracting rate coefficient information, reliable thermodynamic properties ($\Delta_f H^0_{298.15}$, H(T), S(T), G(T), Cp(T)) the reacting species are necessary. $\Delta_f H^0_{298.15}$, H(T), S(T), G(T), Cp(T) are defined as the enthalpy of formation, enthalpy, entropy, Gibbs energy, specific heat at constant pressure. Recently the value of $D^0_{298.15}$(H-OH) = 118.81 ± 0.07 *k*cal mol^{-1} was measured by Ruscic et al.[38] From this new bond dissociation enthalpy of H_2O, $\Delta_f H^0_{298.15}$ (OH) = 8.91 ± 0.07 *k*cal mol^{-1} has been re-established and the differences from the widely used values of Gurvich et al.[39] or JANAF[40] have been discussed in great detail.[38] Previously we had used 9.41 ± 0.05 *k*cal mol^{-1} for $\Delta_f H^0_{298.15}$ (OH), based upon the recommendation of Gurvich et al. The difference of 0.49 *k*cal mol^{-1} from the new value of Ruscic et al. is quite large. Considering the uncertainty in obtaining D^0(H-OH) by Gurvich et al. from spectroscopic measurements and an unambiguous direct measurement of D^0(H-OH) by a photoionization experiment by Ruscic et al., we adopted the new $\Delta_f H^0_{298.15}$ (OH) = 8.91 ± 0.07 *k*cal mol^{-1} by Ruscic et al. and readjusted all thermodynamic data of OH accordingly. The thermodynamic properties of other species in the H_2/O_2 system are unchanged.

While thermodynamic properties of species in a H_2/O_2 system are more or less well established, those of $H_xS_yO_z$ species (HS, HSO, HOSO, HSO_2, and $HOSO_2$) are not. Using

available experimental data and results of theoretical calculations, thermodynamic properties of these species are estimated. Details are in Appendix B.

Computer Simulations for the Determination of Optimal Experimental Conditions

Simulations of experimental results were performed using our custom code. This custom code, utilizing the LSODE[41] integrator, has built-in features for optimization. The accuracy and performance of our code have been extensively tested against the existing chemical kinetics codes.[42, 43]

For the H_2/O_2 system, we adopted a reaction mechanism of 20 elementary reactions that has been tested expansively at various conditions. Then, for the $SO_2/H_2/O_2$ system additional reactions for SO_2 oxidation by H_xO_z species and their rate coefficients were critically reviewed. A reaction mechanism of 35 reactions for this system was composed. A comprehensive but truncated reaction mechanism of 55 reactions for the $SO_2/H_2/O_2$ system is given in Table II.

In order to determine the optimum mixtures and conditions for the experiment a series of sensitivity analyses was performed (see Figures 2(a-c)). In determining the rate coefficients of the reaction,

$$SO_2 + O + M \rightarrow SO_3 + M \qquad \text{(R21)},$$

an O-atom source must be found. In this work O atoms were produced from the H_2/O_2 reaction system. I.e., H_2/O_2 reaction system was perturbed a with small amount of SO_2. The major reactions that consume and produce O atoms in the H_2/O_2 system are

$$O + H_2 \rightarrow OH + H \qquad \text{(R2)}$$

and

$$H + O_2 \rightarrow OH + O \qquad \text{(R1)},$$

respectively. Hence, in the $SO_2/H_2/O_2$ system, R21 would compete with R2. If we use rich H_2/O_2 mixtures, O atoms would be consumed mainly by R2. This restricts us to consider lean H_2/O_2 mixtures only. However, at given jet engine nozzle temperatures (900 - 1200 K), the following reaction will also compete with R1 for H-atoms,

$$H + O_2 + M \rightarrow HO_2 + M \qquad \text{(R9)}$$

Thus, it is also desirable to select reaction mixtures that give the best sensitivity for R21. Sensitivity analyses for the elapsed time to reach the absorption maximum τ_{max} (see the definition in the Results section) were performed using the following baseline H_2/O_2 mixture (without SO_2) with levels of perturbation by SO_2 at $T = 1000$ K, $\rho = 16.0$ μmol cm^{-3}; 0.5% H_2/ 10.0% O_2 ($\Phi = 0.025$), where Φ is the equivalence ratio, 0.15% - 3.0% SO_2/ 0.5% H_2/ 10.0% O_2 ($\Phi = 0.025$)/ Ar. In the baseline mixture, R9, R1, R2, and R3 show sensitivities for τ_{max} in that order. Figure 2(a) shows a sensitivity spectra for 0.5% H_2/ 10.0% O_2/ 89.5% Ar mixture. Figure 2(b) and Figure 2(c) show a sensitivity spectra for the 2.0% SO_2/ 0.5% H_2/ 10.0% O_2/ 87.5% Ar mixture. The sensitivity of R21 was found to be dependent upon the SO_2/H_2 ratio in the mixture. Furthermore, as the SO_2/H_2 ratio is

increased, the sensitivity of R21 and R9 is notably increased together with the relative importance of R21 over R9. Based upon this sensitivity analyses we selected the following five mixtures: for the baseline experiments, 0.5% H_2/ 10.0% O_2/ 89.5% Ar; for perturbation experiments, 0.25%, 1.0%, 2.0%, 3.0% SO_2/ 0.5% H_2/ 10.0% O_2/ Ar and 0.25% SO_2/ 0.25% H_2/ 5.0% O_2/ 94.5% Ar. Further details are shown in Appendix A.

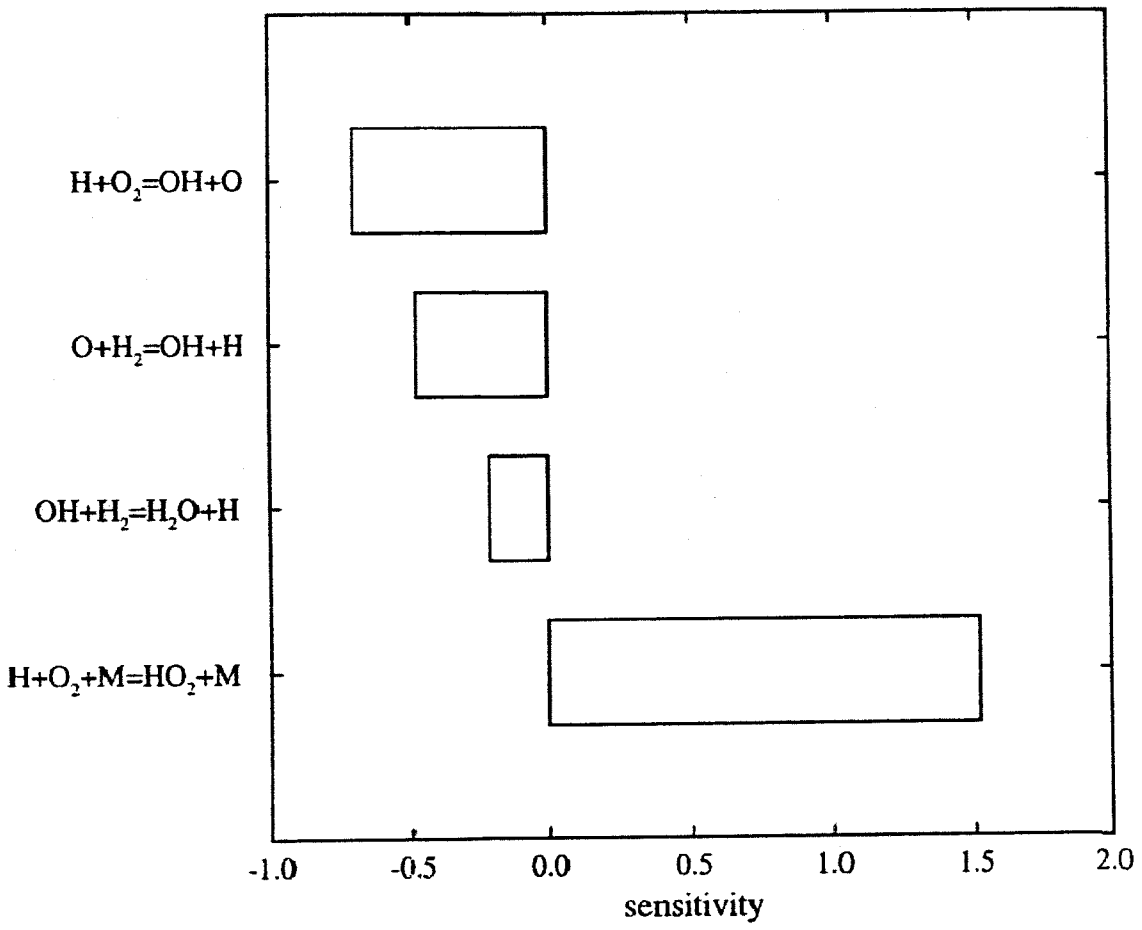

Figure 2(a): Sensitivity of τ_{max} for the baseline mixture (0.5% H_2/ 10.0% O_2/ 89.5% Ar) at $T = 1000$ K and $\rho = 16.0$ μmol cm^{-3}

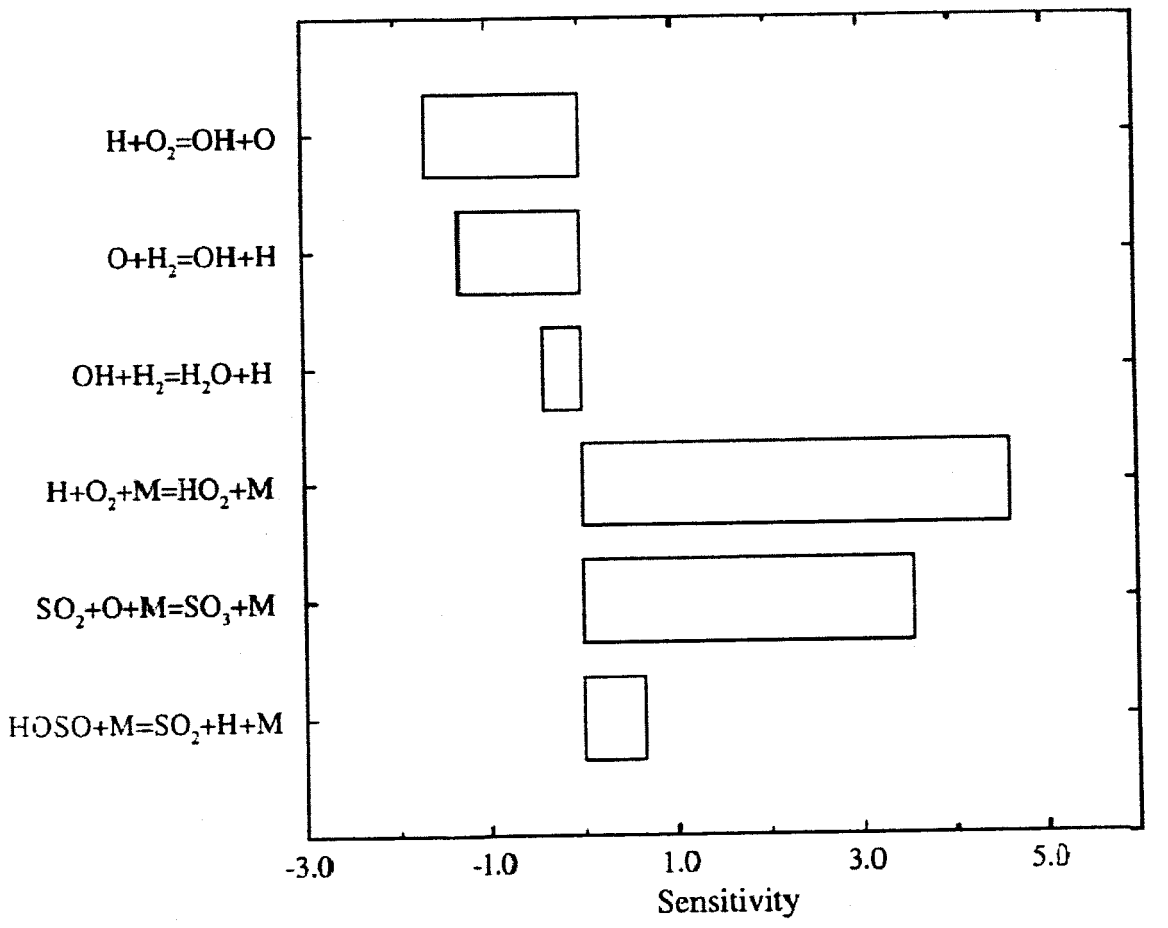

Figure 2(b): Sensitivity of τ_{max} for the mixture (2.0% SO_2/ 0.5% H_2/ 10.0% O_2/ 87.5% Ar) at $T = 1000$ K and $\rho = 16.0$ μmol cm^{-3}

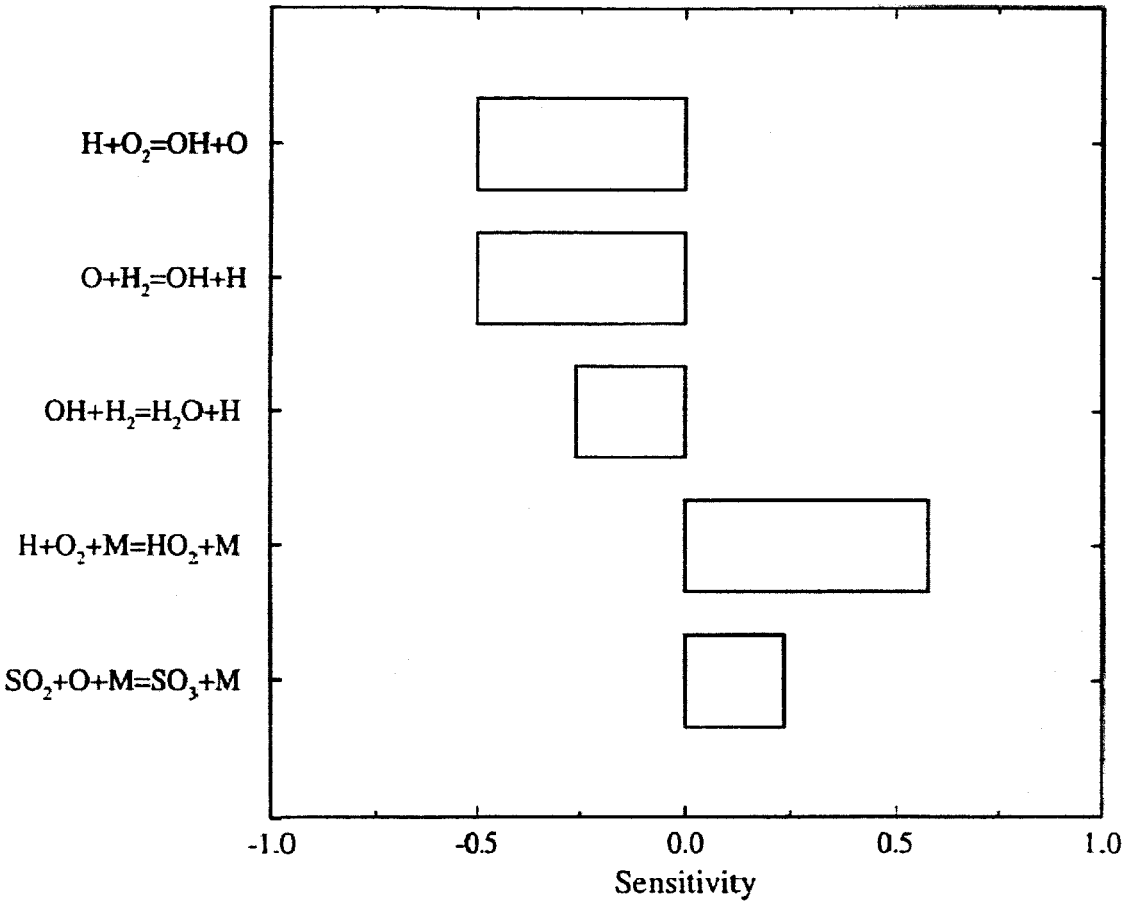

Figure 2(c): Sensitivity of τ_{max} for the mixture (2.0% SO_2/ 0.5% H_2/ 10.0% O_2/ 87.5% Ar) at $T = 1100$ K and $\rho = 16.0$ μmol cm^{-3}

Table II: Reaction Mechanism[a]

	reaction	A	n	Θ	Ref.
1	$H+O_2=OH+O$	6.73E+15	-0.499	8390	37
2	$O+H_2=OH+H$	2.04E+14	0	6972	37
3	$OH+H_2=H+H_2O$	2.16E+08	1.51	1726	37
4	$O+H_2O=OH+OH$	4.51E+04	2.7	7323	37
5	$O+O+M=O_2+M$	1.00E+17	-1	0	37
	Ar,1.0/ H_2,2.9/ O_2,1.2/ H_2O,18.5/[e]				
6	$H+H+M=H_2+M$	6.40E+17	-1	0	37
	Ar,1.0/ H_2,4.0/ H_2O,12.0/ H,26.0/[e]				
7	$H+O+M=OH+M$	6.20E+16	-0.6	0	37
	Ar,1.0/ H_2O,5.0/[e]				
8	$H+OH+M=H_2O+M$	8.40E+21	-2	0	37
	Ar,1.0/ H_2,2.5/ H_2O,16.25/[e]				
9	$H+O_2+M=HO_2+M$	4.57E+18	-1.12	0	37
	Ar,1.0/ O_2,1.33/ H_2,3.33/ H_2O,21.3/SO_2,1.5/[e]				
10	$HO_2+H=OH+OH$	8.40E+13	0	320	37
11	$HO_2+H=H_2+O_2$	2.50E+13	0	350	37
12	$HO_2+H=H_2O+O$	5.00E+12	0	710	37
13	$HO_2+O=O_2+OH$	2.00E+13	0	0	37
14	$HO_2+OH=H_2O+O_2$	2.00E+13	0	0	37
15	$HO_2+HO_2=O_2+H_2O_2$[f]	1.30E+11	0	-820	37
	$HO_2+HO_2=O_2+H_2O_2$[f]	4.20E+14	0	6040	37
16	$H_2O_2+M=OH+OH+M$	1.20E+17	0	22900	37
	Ar,0.67/ O_2,0.78/ H_2O,6.0/[e]				
17	$H_2O_2+H=HO_2+H_2$	1.70E+12	0	1900	37
18	$H_2O_2+H=H_2O+OH$	1.00E+13	0	1805	37
19	$H_2O_2+O=HO_2+OH$	2.80E+13	0	3225	37
20	$H_2O_2+OH=HO_2+H_2O$	1.00E+12	0	0	37
	$H_2O_2+OH=HO_2+H_2O$	5.75E+12	0	4810	37

Table II: Reaction Mechanism[a] (continued)

	reaction	A	n	Θ	Ref.
21	$SO_2+O+M=SO_3+M$	1.30E+24	-2.5	2340	this study
	Ar, 1.0/ O_2,1.3/ SO_2,9.0/[e]				
22	$SO+O+M=SO_2+M$	6.36E+24	-2.6	0	55
	Ar, 1.0/ O_2,1.3/ SO_2,0.0/[e]				
23	$SO+O+SO_2=SO_2+SO_2$	1.88E+27	-3.26	0	55
24	$SO_3+SO=SO_2+SO_2$	1.00E+12	0	2010	45
25	$SO+OH=SO_2+H$	5.20E+13	0	0	45
26	$HOSO(+M)=SO_2+H(+M)$	[b] 1.7E+10	0.8	23600	45
		[c] 1.6E+31	-4.53	24760	45
	$F_c = 0.45$ [d]				
	Ar,1.0/ SO_2,1.5/[e]				
27	$HSO_2(+M)=SO_2+H(+M)$	[b] 2.0E+11	-0.9	9260	45
		[c] 3.5E+25	-3.29	9610	45
	$F_c = 1.0$[d]				
	Ar,1.0/[e]				
28	$SO+O_2=SO_2+O$	6.20E+03	-2.42	1535	45
29	$SO_2+OH=HOSO+O$	3.90E+08	1.89	38250	45
30	$SO_2+OH(+M)=HOSO_2(+M)$	[b] 7.2E+12	0	360	45
		[c] 4.5E+25	-3.3	360	45
	$F_c = 0.29 + 0.64\exp(-T/300)$ [d]				
	Ar,1.0/ O_2,1.5/ SO_2,12.0/[e]				
31	$SO_2+HO_2=SO_3+OH$	1.40E+11	0	3686	see text
32	$SO_2+OH=SO_3+H$	490	2.69	11980	45
33	$HOSO_2+M=SO_3+H+M$	3.20E+16	-0.81	27020	45
	Ar,0.75/ H_2,2.5/ H_2O,12.0/[e]				
34	$SO_3+H=HOSO+O$	2.50E+05	2.92	25310	45
35	$SO_3+O=SO_2+O_2$	1.30E+12	0	3070	56
36	$SO_3+H_2O=H_2SO_4$	8.20E+04	1	-6540	56
37	$HOSO_2+H=SO_2+H_2O$	1.00E+12	0	0	45
38	$HOSO_2+OH=SO_3+H_2O$	1.00E+12	0	0	45
39	$HOSO_2+O=SO_3+OH$	5.00E+12	0	0	45

Table II: Reaction Mechanism[a] (continued)

	reaction	A	n	Θ	Ref.
40	$HOSO_2+O_2=SO_3+HO_2$	7.80E+11	0	330	45
41	$HOSO+H=SO+H_2O$	6.30E-10	6.29	-960	45
42	$HOSO+OH=SO_2+H_2O$	1.00E+12	0	0	45
43	$HOSO+O_2=SO_3+HO_2$	1.00E+12	0	500	45
44	SO+OH+M=HOSO+M	8.00E+21	-2.16	420	45
	Ar,1.0/[e]				
45	HSO+O+M=HOSO+M	6.90E+19	-1.61	800	45
	Ar,1.0/[e]				
46	HSO_2+M=HOSO+M	1.00E+09	1.03	25170	45
		1.70E+35	-5.64	27880	45
	$F_c = 0.44$[f]				
	Ar,1.0/[e]				
47	HSO+O+M=HSO_2+M	1.10E+19	-1.73	-25	45
	Ar,1.0/[e]				
48	SO+H+M=HSO+M	5.00E+15	0	0	45
	Ar,1.0/[e]				
49	HSO+H=HS+OH	4.90E+19	-1.86	785	45
50	HSO+H=SO+H_2	1.00E+12	0	0	45
51	HSO+O=SO_2+H	4.50E+14	-0.4	0	45
52	HSO+O=SO+OH	1.40E+13	0.15	150	45
53	HSO+OH=SO+H_2O	1.70E+09	1.03	205	45
54	HSO+OH=HOSO+H	5.30E+07	1.57	1890	45
55	HSO+O_2=SO+HO_2	1.00E+12	0	0	45

[a] Rate coefficients are in the form, $k = AT^n \exp(-\Theta/T)$. Units are K, cm, mol, and s.

[b] k_∞

[c] k_0

[d] Fall-off correction parameters.

[e] Collision efficiencies.

[f] Duplicated reaction.

Results

Figure 3 shows a typical OH absorption profile. The reflected shock passage (time zero) is shown in the form of a schlieren peak. The initial SO_2 absorption is clearly seen prior to the schlieren peak. After an induction period the absorption increases rapidly due to the exponential growth of [OH] by chain-branching reactions (see Discussion). After the peak, the absorption diminishes as the OH attains its equilibrium concentration.

SO_2 molecules along with OH radicals absorb 310 nm UV light. Since, in this work, absorption profiles are due from OH radicals produced and SO_2 molecules present, it was necessary to measure the absorption coefficients of SO_2. Beer's Law was utilized in the calculation of the absorption coefficients of SO_2: $I/I_0 = \exp(-\sigma_{SO2} \times C_{SO2} \times l)$, where I_0 and I are, respectively, initial and transmitted light intensity and σ_{SO2}, C_{SO2} and l are base 'e' absorption coefficient, concentration of SO_2 and light path length, respectively. The mean room temperature value measured by the pump-fill-pump method was $(7.0 \pm 1.7) \times 10^4$ cm^2 mol^{-1}. This value is about 30% smaller than the spectroscopic measurement of Vandaele et al.[44] At high temperatures, the flat portion of the signal behind the reflected shock, but before the visible rise of absorption, was taken as the transmitted light intensity (I). The initial light intensity (I_0) was estimated by taking into account the room temperature absorption. Figure 4 shows the high temperature absorption coefficients of SO_2. A temperature dependent fit for the high temperature data was avoided because of the

narrow temperature range of the data (960 - 1150 K). Instead, a temperature dependent fit was developed using the mean value of the high temperature data at 1050 K, 1.1×10^5 cm^2 mol^{-1} and the room temperature value:

$$\sigma_{SO2} = 1.3 \times 10^5 \exp(-180\ \mathrm{K}/T)\ \mathrm{cm}^2\ \mathrm{mol}^{-1}.$$

From an experimental absorption profile, the following set of observables were obtained: an initial SO_2 absorption after the reflected shock passage, $A_{SO2} = 1 - I_{SO2}/I_0$, a maximum absorption, $A_{max} = (1 - I/I_0)_{max}$, and characteristic times (τ_{25}, τ_{50}, τ_{75} and τ_{max}). Evaluation of τ_{max}, time to reach A_{max}, is straight forward (see Figure 3).

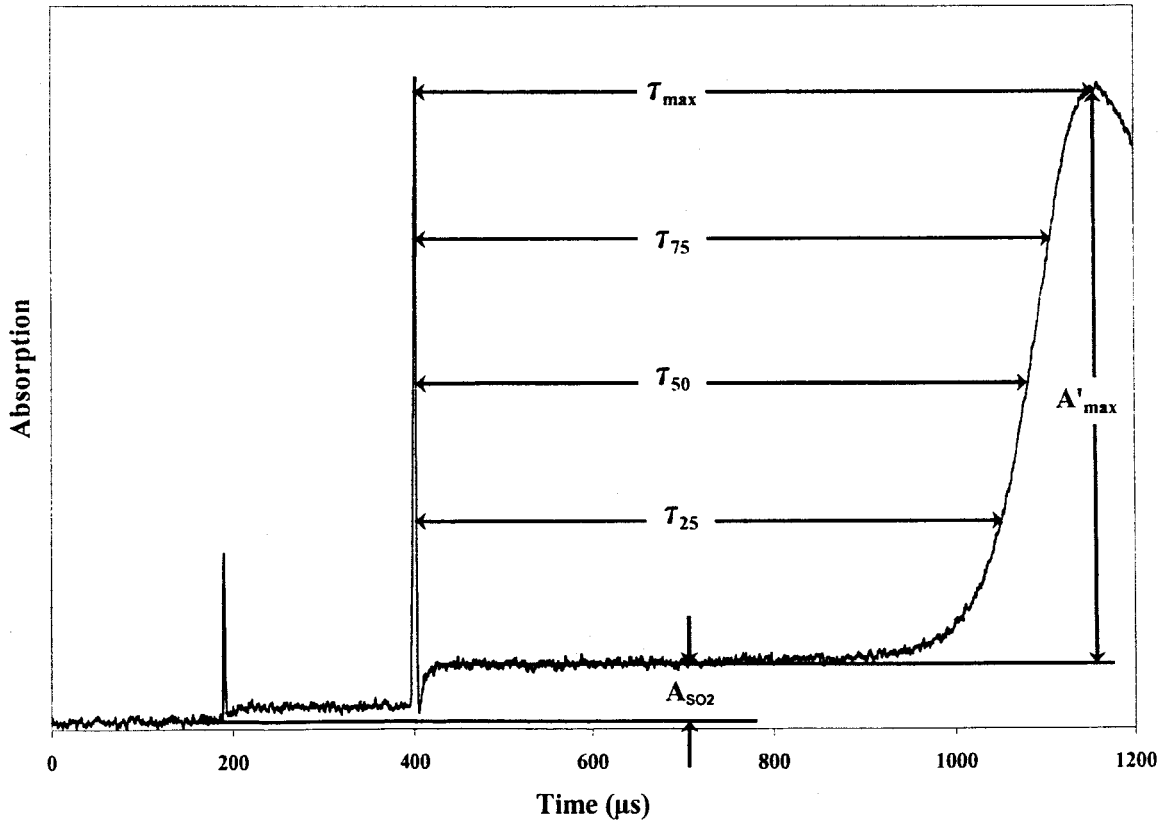

Figure 3: Deduction of Experimental Observables

For τ_{25}, τ_{50} and τ_{75}, however, due to the considerably large A_{SO2} and sometimes relatively small A_{max}, a subtracted absorption signal (total absorption – A_{SO2}) was used. Then τ_{25}, τ_{50} and τ_{75} are defined as times to reach 25%, 50% and 75% of the value of A'_{max} = $A_{max} - A_{SO2}$. Figures 5(a) and 5(b) show τ_{max} and τ_{25} measured for the perturbed mixtures, 0.25%, 1.0%, 2.0% and 3.0% SO_2/ 0.5% H_2/ 10.0% O_2/ 87.5, 86.5% Ar together with the values for the baseline mixture, 0.5% H_2/ 10.0% O_2/ 89.5% Ar. Throughout all experiments, densities were kept nearly the same between the baseline and perturbed experiments. Although direct comparison of characteristic times, except for τ_{max}, between the baseline and perturbed mixtures gives some bias, it is clearly shown that perturbation with SO_2 prolongs the characteristic times. Furthermore, the perturbation effect on characteristic times increases as the SO_2/H_2 ratio increases and the temperature decreases. This increase of characteristic times is due mainly to the depletion of O atoms by R21, so the H-atom production rate by R2 is reduced. This, in turn, reduces the branching rate of R1.

Using the reaction mechanism given in Table II (see the section: Computer Simulations to Determine Optimal Experimental Conditions), computer simulations have been performed to determine the rate coefficients of Reaction 21, $SO_2 + O + M \rightarrow SO_3 + M$, that is the most sensitive SO_x reaction to the temporal absorption profile (experimental observables). For a given experimental condition, matching these observables is equivalent to the simulation of a whole experimental profile. The rise of the absorption signal from A_{SO2} is originated from OH production because the σ_{OH} values are approximately 2 orders of magnitude higher than σ_{SO2}. In the simulation, the $k_{21,0}$ value was varied and the absorption coefficients of SO_2 and OH were adjusted appropriately within ±35% of their

nominal values — this adjustment is acceptable because the coupling of A_{SO2} and A_{max} to the kinetics is either absent or weak (self-calibration). Excellent matches to the experimental profiles could be obtained by additional minor adjustment of k_{14}(HO_2 + OH → H_2O + O_2). A simulated absorption profile is shown in Figure 3. The resulting $k_{21,0}$ values are plotted in Figure 6 together with the fall-off values, calculated at our experimental conditions using Mueller et al.'s[45] rate coefficient expressions for $k_{21,0}$/[M], $k_{21,\infty}$and interpolation parameter(s). Experimental conditions, measured observables and the rate coefficients determined for individual experiments are given in Table III.

Table III: Experimental Conditions and Results

T_5 (K)	P_5 (atm)	$\rho_5 \times 10^5$ (μmol cm^3)	A_{max}	τ_{max} (μs)	τ_{75} (μs)	τ_{50} (μs)	τ_{25} (μs)	A_{SO2}	$(k_{21,0}/[M])/10^{15}$ (cm^{6}mol^{-2}s^{-1})	$k_{21,0}/10^{10}$ (cm^{3}mol^{-1}s^{-1})
0.25% SO_2/ 0.25% H_2/ 5.0% O_2/ 94.5% Ar										
1003	1.329	1.615	0.162	3070	2766	2626	2480	0.044	3.97	6.63
1027	1.332	1.581	0.199	2245	1949	1824	1685	0.054	3.95	6.47
1071	1.390	1.581	0.288	1350	1176	1096	1005	0.056	3.35	5.49
1053	2.579	2.985	0.266	1727	1499	1387	1275	0.130	4.02	12.4
1062	2.606	2.990	0.294	1475	1279	1183	1085	0.129	3.95	12.2
1068	2.627	2.998	0.314	1314	1133	1053	965	0.133	3.84	11.9
1068	2.635	3.006	0.224	1296	1105	1024	950	0.092	3.78	11.8
0.25% SO_2/ 0.5% H_2/ 10.0% O_2/ 89.25% Ar										
961	1.259	1.596	0.221	3238	2943	2806	2655	0.046	4.29	7.19
961	1.257	1.594	0.227	3194	2958	2816	2658	0.048	4.17	6.98
968	1.279	1.611	0.202	2890	2593	2442	2300	0.044	4.31	7.29
971	1.272	1.596	0.205	2679	2421	2286	2147	0.041	4.32	7.25
976	1.284	1.604	0.199	2447	2161	2027	1887	0.045	3.56	6.00
980	1.309	1.627	0.182	2428	2099	1948	1783	0.045	4.18	7.15
993	1.319	1.619	0.203	1815	1587	1490	1378	0.044	3.60	6.12
1000	1.314	1.600	0.224	1634	1407	1313	1210	0.044	4.27	7.18
1003	1.320	1.605	0.236	1510	1305	1220	1124	0.044	3.97	6.69
1016	1.352	1.627	0.234	1289	1104	1027	946	0.045	3.76	6.41
1.0% SO_2/ 0.5% H_2/ 10.0% O_2/ 88.5% Ar										
991	1.297	1.595	0.373	2895	2600	2471	2303	0.19	4.13	7.32
995	1.288	1.578	0.360	2966	2651	2493	2309	0.175	4.69	8.22
996	1.311	1.604	0.368	2585	2337	2212	2072	0.193	4.18	7.44
1003	1.325	1.611	0.328	2349	2087	1957	1799	0.182	4.27	7.62
1004	1.324	1.608	0.357	2102	1858	1737	1609	0.176	3.57	6.37
1007	1.313	1.590	0.341	2133	1887	1780	1623	0.177	4.27	7.54
1014	1.331	1.600	0.373	1802	1563	1460	1347	0.197	3.69	6.56
1023	1.375	1.638	0.379	1513	1323	1236	1145	0.201	3.77	6.85
1040	1.394	1.633	0.413	1262	1095	1023	944	0.204	4.26	7.72
1053	1.418	1.641	0.447	1055	910	851	786	0.200	4.30	7.84
1056	1.430	1.650	0.466	994	871	820	761	0.194	4.29	7.86
2.0% SO_2/ 0.5% H_2/ 10.0% O_2/ 87.5% Ar										
1014	1.353	1.627	0.554	2891	2642	2499	2317	0.385	3.97	7.69
1014	1.357	1.631	0.566	2657	2370	2231	2055	0.407	3.44	6.67
1018	1.364	1.632	0.527	2671	2292	2114	1907	0.402	3.54	6.88
1021	1.459	1.742	0.550	2457	2190	2059	1900	0.403	3.49	7.24
1026	1.340	1.591	0.515	2100	1815	1675	1529	0.376	3.46	6.56
1027	1.373	1.630	0.577	1996	1756	1646	1525	0.415	3.45	6.69
1031	1.350	1.597	0.511	1946	1642	1528	1404	0.373	3.54	6.73
1036	1.339	1.575	0.511	1805	1614	1510	1389	0.352	4.20	7.88
1045	1.380	1.607	0.443	1493	1289	1185	1061	0.322	3.30	6.31
1045	1.411	1.646	0.549	1539	1348	1257	1158	0.392	4.05	7.93
1047	1.376	1.602	0.552	1282	1125	1048	966	0.365	3.24	6.18
1047	1.375	1.600	0.467	1489	1297	1203	1093	0.335	3.96	7.54
1051	1.374	1.593	0.582	1248	1093	1041	932	0.404	3.42	6.49
1055	1.418	1.637	0.560	1435	1241	1158	1064	0.393	4.80	9.36
1056	1.393	1.608	0.583	1155	1005	938	865	0.410	3.43	6.56
1057	1.389	1.601	0.556	1237	1090	1010	934	0.372	4.22	8.04
1061	1.442	1.656	0.573	1134	997	933	859	0.380	4.02	7.91

Table III: Experimental Conditions and Results (continued)

T_5 (K)	P_5 (atm)	$\rho_5 \times 10^5$ (μmol cm^3)	A_{max}	τ_{max} (μs)	τ_{75} (μs)	τ_{50} (μs)	τ_{25} (μs)	A_{SO2}	$(k_{21,0}/[M])/10^{15}$ (cm^{6}mol^{-2}s^{-1})	$k_{21,0}/10^{10}$ (cm^{3}mol^{-1}s^{-1})
1068	1.440	1.643	0.654	1052	906	844	781	0.449	4.15	8.11
1068	1.393	1.590	0.634	1057	911	854	786	0.430	4.38	8.28
1069	1.406	1.603	0.512	1157	994	917	826	0.341	4.32	8.24
1072	1.395	1.586	0.636	1001	871	813	751	0.419	4.27	8.07
1073	1.400	1.591	0.632	982	840	781	716	0.421	3.83	7.26
1084	1.426	1.604	0.671	791	676	627	576	0.418	3.08	5.87
1085	1.417	1.591	0.562	925	799	742	680	0.343	3.59	6.80
1090	1.432	1.601	0.586	877	759	703	643	0.360	3.46	8.27
1091	1.434	1.601	0.555	839	723	678	611	0.339	3.63	6.92
1097	1.458	1.620	0.690	767	646	603	556	0.434	3.84	7.40
1097	1.426	1.531	0.636	759	651	604	553	0.374	3.73	7.02
1106	1.438	1.584	0.639	694	596	552	503	0.368	3.82	8.09
1117	1.456	1.588	0.720	578	496	459	421	0.400	3.55	6.70
1124	1.481	1.606	0.722	590	514	479	439	0.397	4.11	7.86
1131	1.485	1.600	0.722	546	468	432	398	0.389	3.97	7.56
1147	1.530	1.625	0.759	440	377	349	320	0.391	3.65	7.05
			3.0% SO_2/ 0.5% H_2/ 10.0% O_2/ 86.5% Ar							
1033	1.446	1.706	0.554	2710	2443	2300	2107	0.445	3.52	7.62
1036	1.452	1.709	0.560	2696	2330	2178	1975	0.453	3.48	7.54
1040	1.465	1.716	0.552	2602	2253	2098	1921	0.447	3.74	8.16
1045	1.428	1.665	0.657	2445	2197	2049	1838	0.522	4.38	9.26
1051	1.442	1.673	0.548	2018	1703	1566	1421	0.451	3.64	7.36
1067	1.407	1.607	0.664	1580	1380	1287	1178	0.552	4.44	9.68
1068	1.415	1.615	0.547	1323	1119	1081	929	0.429	3.34	6.84
1084	1.446	1.626	0.569	1015	871	800	730	0.434	3.42	7.06
1094	1.419	1.580	0.617	827	712	660	599	0.431	3.44	6.26
1101	1.487	1.646	0.590	879	756	693	630	0.434	4.10	8.57
1118	1.450	1.580	0.759	675	579	535	487	0.546	3.95	7.93
1124	1.458	1.582	0.681	591	511	472	431	0.438	3.42	6.86
1131	1.443	1.555	0.705	562	477	443	405	0.433	3.24	6.40
1152	1.473	1.559	0.561	435	376	349	318	0.317	3.16	6.26

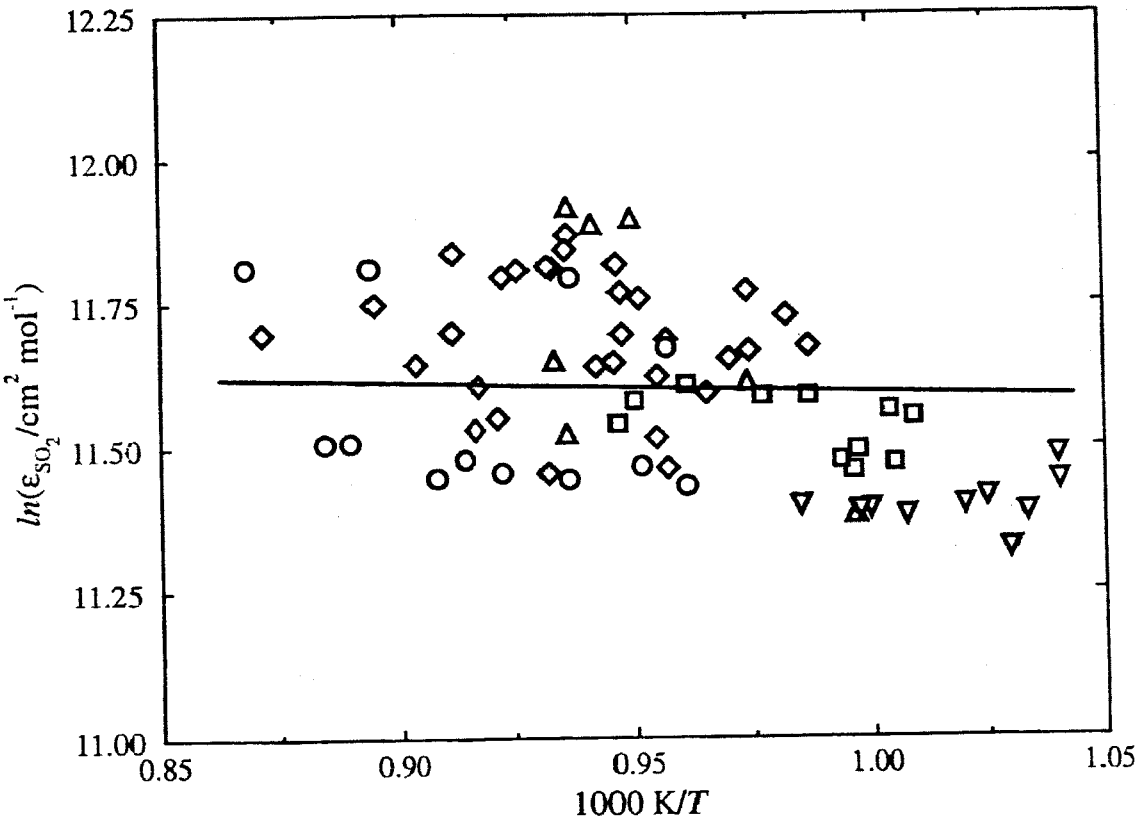

Figure 4: Base 'e' absorption coefficients of SO_2 at 310 nm. Symbols are: △, 0.25% SO_2/ 0.25% H_2/ 5.0% O_2/ 94.5% Ar; ▽, 0.25% SO_2/ 0.5% H_2/ 10.0% O_2/ 89.25% Ar; □, 1.0% SO_2/ 0.5% H_2/ 10.0% O_2/ 88.5% Ar; ◊, 2.0% SO_2/ 0.5% H_2/ 10.0% O_2/ 87.5% Ar: ○, 3.0% SO_2/ 0.5% H_2/ 10.0% O_2/ 86.5% Ar. The least squares fit is $\epsilon_e(SO_2) = 1.3 \times 10^{15} \exp(-180\ \mathrm{K}/T)\ \mathrm{cm}^2\ \mathrm{mol}^{-2}$.

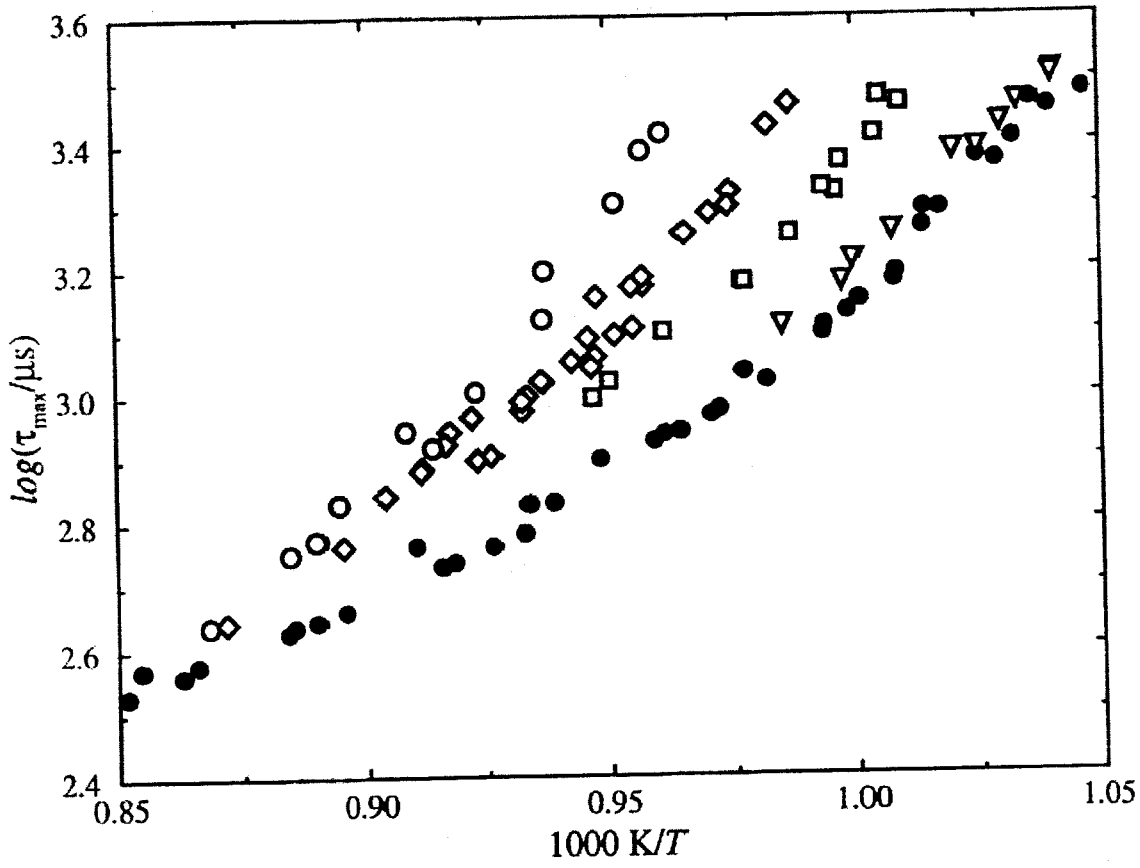

Figure 5(a): Measured τ_{max} values of the baseline and SO_2-perturbed mixtures. Symbols are: ●0.5% H_2/ 10.0% O_2/ 89.5% Ar; ▽, 0.25% SO_2/ 0.5% H_2/ 10.0% O_2/ 89.25% Ar; □, 1.0% SO_2/ 0.5% H_2/ 10.0% O_2/ 88.5% Ar; ◊, 2.0% SO_2/ 0.5% H_2/ 10.0% O_2/ 87.5% Ar: ○, 3.0% SO_2/ 0.5% H_2/ 10.0% O_2/ 86.5% Ar.

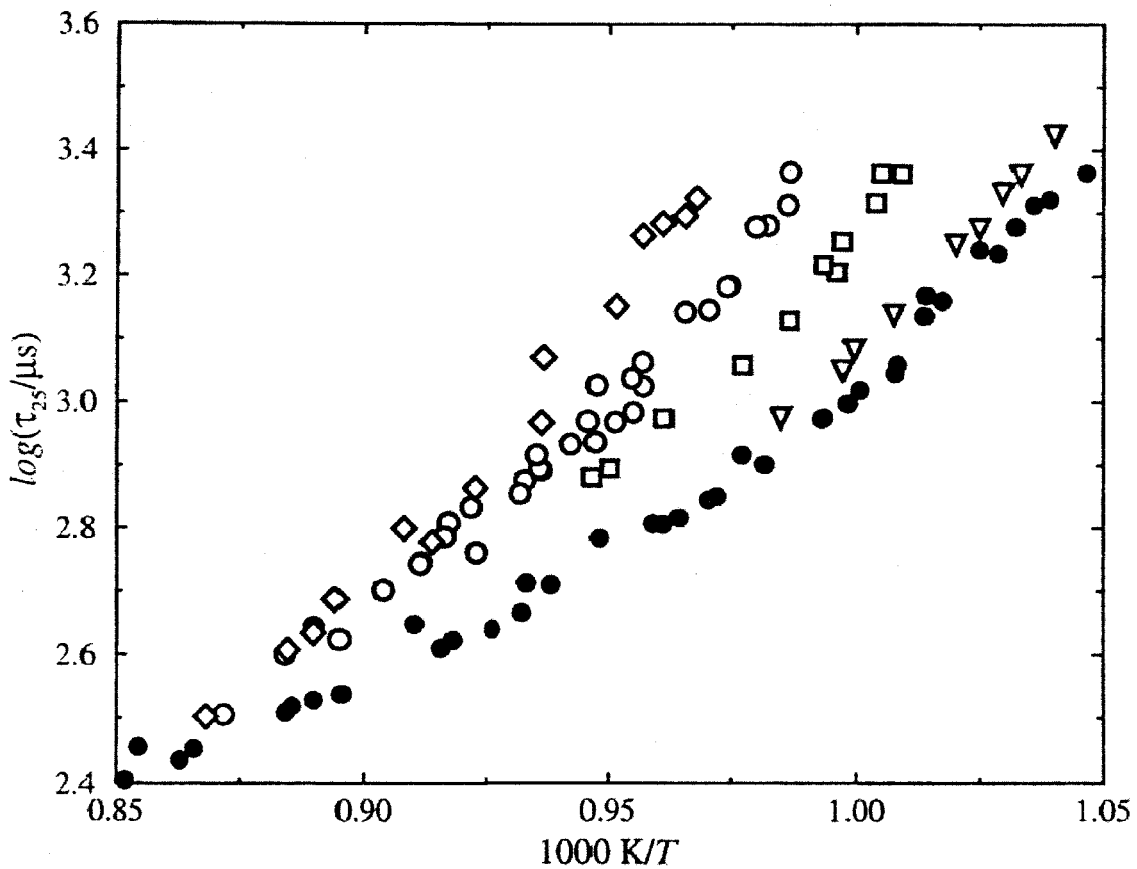

Figure 5(b): Measured τ_{25} values of the baseline and SO_2-perturbed mixtures. Symbols are: •0.5% H_2/ 10.0% O_2/ 89.5% Ar; ▽, 0.25% SO_2/ 0.5% H_2/ 10.0% O_2/ 89.25% Ar; □, 1.0% SO_2/ 0.5% H_2/ 10.0% O_2/ 88.5% Ar; ◊, 2.0% SO_2/ 0.5% H_2/ 10.0% O_2/ 87.5% Ar: ○, 3.0% SO_2/ 0.5% H_2/ 10.0% O_2/ 86.5% Ar.

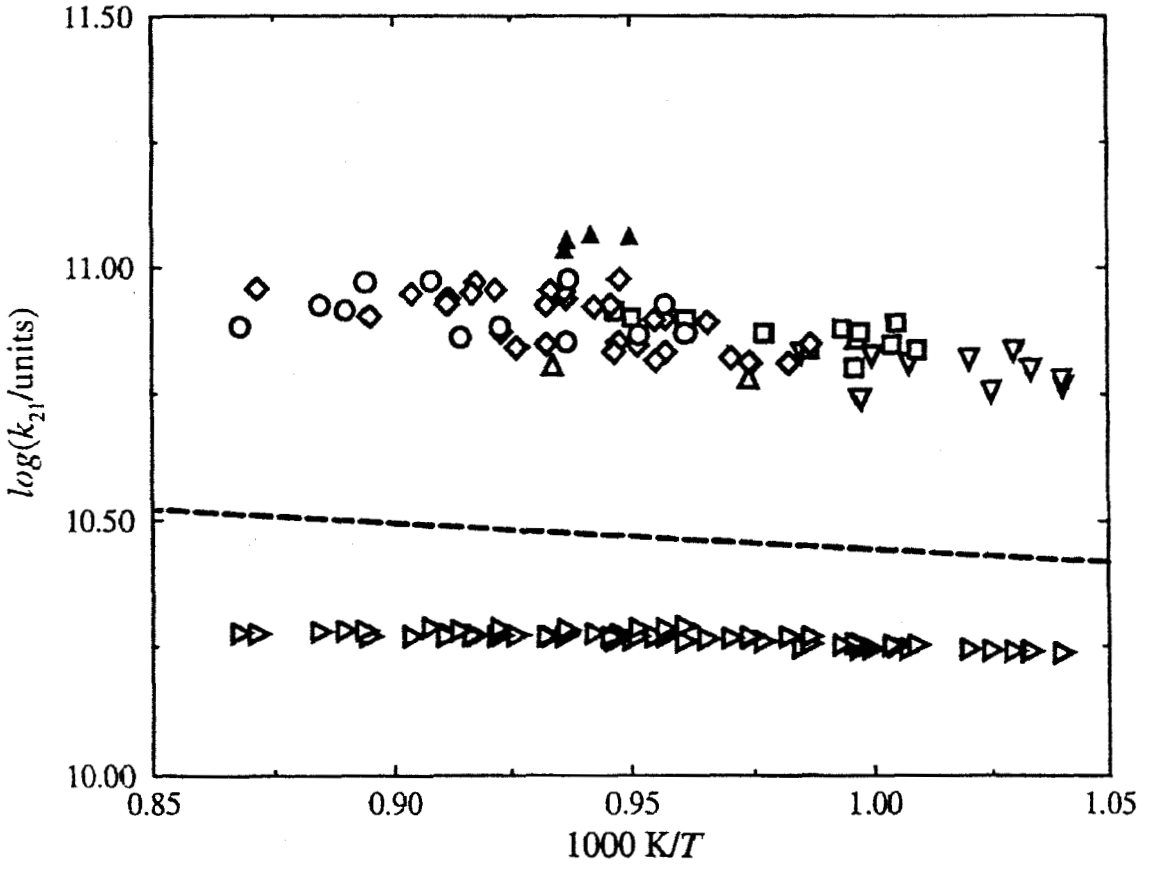

Figure 6: The comparison of our $k_{21,0}$ values with Mueller et al.'s $k_{21,\text{eff}}$ computed at our conditions. Symbols are: △, 0.25% SO_2/ 0.25% H_2/ 5.0% O_2/ 94.5% Ar, ρ = x-axes μmol cm^{-3}; ▲, 0.25% SO_2/ 0.25% H_2/ 5.0% O_2/ 94.5% Ar, ρ = x-axes μmol cm^{-3}; ▽, 0.25% SO_2/ 0.5% H_2/ 10.0% O_2/ 89.25% Ar, ▷, $k_{21,\text{eff}}$ values of Mueller et al. – –, $k_{21,\infty}$ values of Mueller et al. Note the linear increase of $k_{21,0}$ values with density (△,▲) in our measurements.

Discussion

As can be seen in Figure 6, the $k_{21,0}$ values show a slightly negative temperature dependence at $T = 960$ - 1150 K and $\rho_{av} = 16.1$ μmol cm^{-3}. When the density was increased to $\rho_{av} = 30.0$ μmol cm^{-3}, a near proportional increase of $k_{21,0}$ was observed. This is a clear indication that in our experimental conditions the title reaction is in the low pressure limit. Therefore, at each experimental condition, $k_{21,0}$/[M] was obtained simply by scaling $k_{21,0}$ with the corresponding collision - efficiency - corrected density, $[M] = \rho \times [1 + x_{O2}(\epsilon_{O2} - 1) + x_{SO2}(\epsilon_{SO2} - 1)]$. The collision efficiencies are $\epsilon_{O2} = 1.3$ and $\epsilon_{SO2} = 9.0$. The $k_{21,0}$/[M] values obtained in this manner are listed in Table III and are also plotted in Figure 7. Again, a slightly negative temperature dependence is apparent. However, because of the large uncertainties in the determined rate coefficients (see below) and the very narrow temperature range employed, it is rather risky to present a temperature dependent rate coefficient expression. Therefore, we decided to give a mean value

$$k_{21,0}/[M] = 3.9 \times 10^{15} \text{ cm}^6 \text{ mol}^{-2} \text{ s}^{-1}$$

over the range of $T = 960$ - 1150 K and $\rho = 16$ - 30 μmol cm^{-3} ($P = 1.25$ - 2.65 atm).

In the course of rate coefficient derivation by computer simulation using our base reaction mechanism, we realized that high $k_{21,0}$ values were associated with small initial SO_2 concentration in the mixtures at comparable temperature and density conditions. This

was a clue of inadequacy of the base mechanism because rate coefficients must not be dependent upon the mixture compositions used. Three plausible causes for this phenomenon were speculated: (a) the actual initial SO_2 concentration in the mixture is smaller than the nominal due to the adsorption of SO_2 on the inner surfaces of the mixing tank and shock tube; (b) the SO_2 self-reaction, $SO_2 + SO_2 \rightarrow$ products; and (c) reaction(s) not considered in the mechanism.

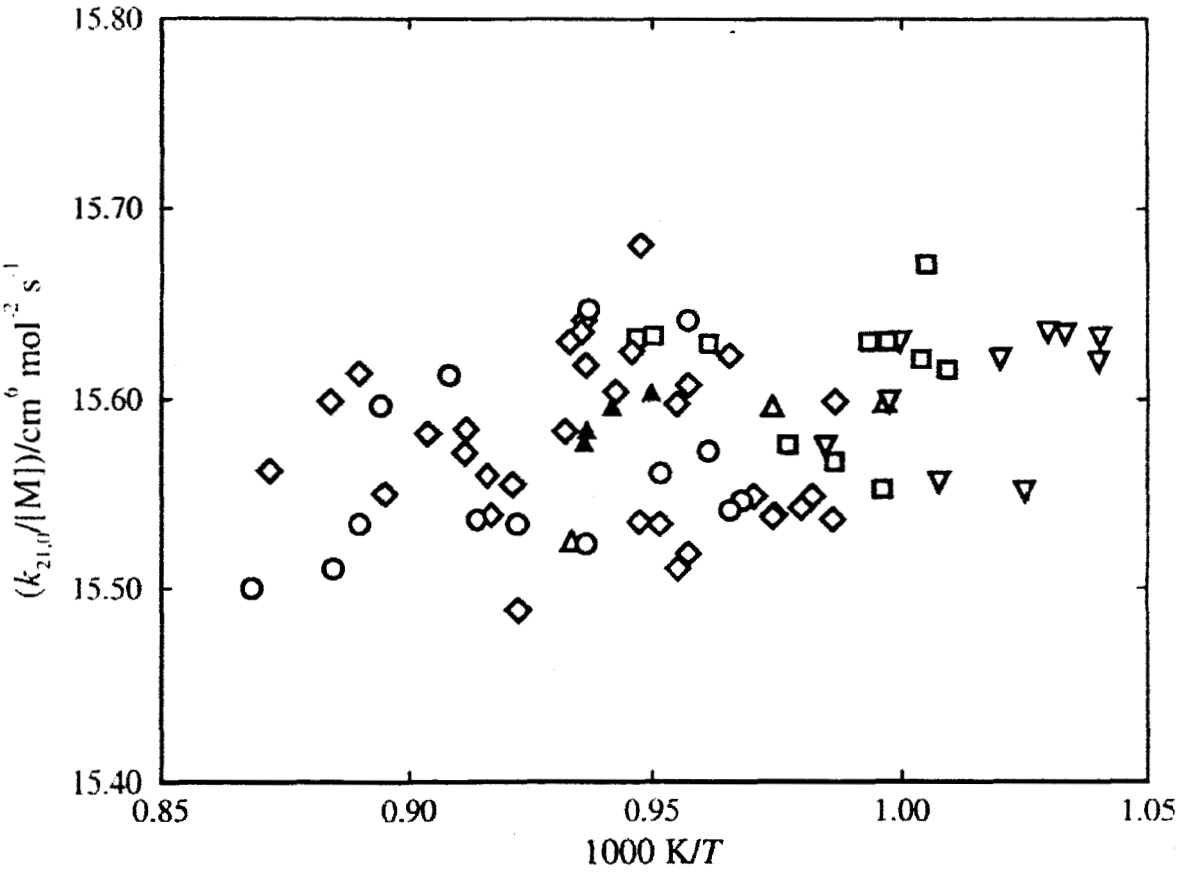

Figure 7: The $k_{21,0}/[M]$ values determined in this study. Symbols are: △, 0.25% SO_2/ 0.25% H_2/ 5.0% O_2/ 94.5% Ar, ρ = x-axes μmol cm^{-3}; ▲, 0.25% SO_2/ 0.25% H_2/ 5.0% O_2/ 94.5% Ar, ρ = x-axes μmol cm^{-3}; ▽, 0.25% SO_2/ 0.5% H_2/ 10.0% O_2/ 89.25% Ar. The mean value is 3.9×10^{15} cm^6 mol^{-2} sec^{-1} over the temperature and density range of T = 960 - 1150 K and ρ = 16 - 30 μmol cm^{-3} (P = 1.25 - 2.65 atm), respectively with uncertainty limits of ±30.

For case (a), if adsorption is significant, reduction of the initial SO_2 concentration would be greater for the leaner SO_2 mixtures and would have resulted in the shortening of the measured characteristic times. Simulations for the experimental absorption profiles with reduction of SO_2 by the same amount from its initial (nominal) concentration, however, did not resolve the inter-dependency of $k_{21,0}$ on SO_2 composition of the mixture. Depletion of SO_2 due to adsorption, if there is any, should be reflected on the absorption coefficients of SO_2. Perusal of Figure 4 does not show any noticeable trend in absorption coefficients. Thus the possibility of case (a) is ruled out.

For case (b), depletion of SO_2 by itself-reaction would increase with initial SO_2 concentration in the mixture and will result in shortening of the characteristic times. Thus, if we include this reaction in the reaction mechanism, we would expect first, higher $k_{21,0}$ values through shortening of the characteristic times than those without this reaction and second, the increase in $k_{21,0}$ values would be larger in the richer SO_2 mixtures. However, what we observed was the following: for leaner SO_2 mixtures there were negligible changes in $k_{21,0}$ and, for richer SO_2 mixtures, the was a decrease of the optimized $k_{21,0}$ values via the lengthening of the characteristic times. Explanation for this unexpected outcome can be given by H-atom flux. In the H_2/O_2 system, after initiation, H atoms are consumed by $H + O_2 \rightarrow OH + O$ (R1, chain branching) and $H + O_2 + M \rightarrow HO_2 + M$ (R9, chain termination), and are produced by $O + H_2 \rightarrow OH + H$ (R2, chain propagation) and $OH + H_2 \rightarrow H_2O + H$ (R2, chain propagation). SO_2 perturbation alters H- and O-atom flows by diverting H and O atoms to $SO_2 + O + M \rightarrow SO_2 + M$ (R21) and $HOSO + M \leftarrow SO_2 + H + M$ (R-26) and $SO_2 + OH \leftarrow SO_3 + H$ (R-32). Hence the inclusion of SO_2 self-reaction lowers mainly the reaction rates of R21, R –32, R3 and then of R1. As a result, longer characteristic times

and lower $k_{21,0}$ were obtained and the discrepancies of $k_{21,0}$ values from different initial SO_2 composition mixtures are widened. Therefore SO_2 self-reaction is not included in the base mechanism.

For case (c), we considered R31, $SO_2 + HO_2 \rightarrow SO_3 + OH$ ($\Delta_r H_{298.15} = -17.6$ *k*cal mol^{-1}), since considerably large amounts of HO_2 are always present in our reaction system. A recent compilation of kinetic data[46] listed this reaction without specifying its products. Comparing the similarities among $CH_3 + HO_2 \rightarrow CH_3O + OH$, $NO_2 + HO_2 \rightarrow NO_3 + OH$ and the above reaction, we assigned SO_2 and OH as products. This reaction effectively converts the relatively unreactive HO_2 radical to reactive OH. Because the reaction rate of R31 increases with SO_2 concentration in a mixture, it was expected that inclusion of R31 would bring agreement in $k_{21,0}$ values from different mixtures by reducing the characteristic times with different degrees. Currently, no rate coefficient information is available for this O-atom transfer reaction in our temperature range. The recommended upper limit at room temperature[47] is 6×10^5 cm^3 mol^{-1} s^{-1}. At the middle of our temperature range, $T = 1050$ K, we estimated k_{31} such that $k_{21,0}$ values from different mixtures agree within 30% ($k_{31} = 4.2 \times 10^9$ cm^3 mol^{-1} s^{-1}). An Arrhenius fit was then made with the room temperature value: $k_{31} = 1.4 \times 10^{11} \exp(-3680\ K/T)$ cm^3 mol^{-1} s^{-1}. Although this reaction is exothermic, a 7.3 *k*cal mol^{-1} of activation energy is not unreasonable for S-O bond formation and O-O bond breaking reaction. Nevertheless, experimental rate coefficient measurements of this reaction at high temperatures will be highly beneficial.

All possible uncertainties in our $k_{21,0}$ values are estimated below. Since the title reaction is sensitive only to the characteristic times (not to OH growth rate), an impurity

effect that could influence the derivation of $k_{21,0}$ is considered first. The presence of H atoms from sources other than the initiation reaction, $HO_2 + H \leftarrow H_2 + O_2$ (R –11) would enhance the reaction rate of R1 to shorten the characteristic times. Thus, higher $k_{21,0}$ values would be expected. The effects of H-atom impurity were studied by either increasing k_{11} by a factor of 5 or injecting into the system $[H]_0 = 0.1$ ppb that is about an order of magnitude higher concentration than the early stage H atoms produced by R –11. Regardless of the method of adding H atoms, the $k_{21,0}$ values were increased by 10% with a 3% $SO_2/H_2/O_2$/Ar mixture and about 50% with a 0.25% $SO_2/H_2/O_2$/Ar mixture. The reason for a smaller increase with higher SO_2 composition mixtures is that some portion of H atoms are drained through the reverse of R –26 ($HOSO + M \leftarrow SO_2 + H + M$). Hence we estimated a factor of 2 uncertainty in $k_{21,0}$ owing to the possible presence of impurity as H atoms.

The influence of the uncertainties in other reaction rate coefficients on the determination of $k_{21,0}$ is examined next. As seen in the sensitivity figures, R9 ($H + O_2 + M \rightarrow HO_2 + M$) exhibits the largest sensitivity. Despite the numerous reports on $k_{9,0}$, only two experimental measurements are available in the temperature range of this study (960 - 1150 K); that of Gutman et al.[48] and of Hwang et al.[37] While $k_{9,0}$ of Gutman et al. are the largest at $T > 950$ K, those of Hwang et al. are generally in good agreement with the previous measurements. So, we varied the rate coefficients of Hwang et al. by ±30% (given uncertainty limits) and examined the effects on $k_{21,0}$. The resulting changes of 40% in $k_{21,0}$ led us to put a maximum uncertainty of ±50% on $k_{21,0}$ due to the coupling between R21 and R9.

In the presence of SO_2, H atoms formed in the H_2/O_2 system are also consumed by R –26 (HOSO + M ← SO_2 + H + M). For R –26, Baulch et al.[49] assumed HSO_2 as the product and recommended $k_{-26}/[M] = 5.1 \times 10^{15}$ cm^6 mol^{-2} s^{-1} at T = 1660 - 2120 K, based upon the Kallend's study[50] of SO_2 doped $H_2/O_2/N_2$ flame at atmospheric pressure while ab initio calculations by Binns and Marshall[51] gave $k_{-26}/[M] = 1.12 \times 10^{16} \exp(-6300\ K/T)$ cm^6 mol^{-2} s^{-1} at $T \geq 700$ K. Binns and Marshall's value at T = 2000 K is an order of magnitude smaller than Baulch et al.'s recommendation. The reason for the large discrepancy supplied by Binns and Marshall was the assumed high collision efficiencies of the third bodies and/or overestimation of their ab initio barrier. In the present study, $k_{26,0}/[M]$, $k_{26,\infty}$ and fall-off parameter(s) needed for generation of the pressure dependent rate coefficients were taken from a recent theoretical study of Goumri et al.[52] At T = 2000 K and P = 1 atm, the fall-off value (k_{-26}) of Goumri et al. is, respectively, 2.5 times smaller and 4 times larger than the low pressure limit values ($k_{-26,0}$) of Baulch et al. and Binns and Marshall. On this basis, we multiplied the k_{-26} values of Goumri et al. by 3 and 0.1 and reoptimized $k_{21,0}$. The matches to the experimental profiles were not as good as before and the reoptimized $k_{21,0}$ values varied from +10% to –30% from the original ones. The coupling of the title reaction with R32 (SO_2 + OH → SO_3 + H) and with the autocatalytic O-atom destruction reaction, R35 (SO_3 + O → SO_2 + O_2), is also investigated. The rate coefficient expression, $k_{32} = 4.9 \times 10^2\ T^{2.69} \exp(-11980\ K/T)$ cm^3 mol^{-1} s^{-1} was from the Quantum Rice, Ramsperger and Kassel estimates (QRRK) by Chiang.[53] A factor of five variation of k_{32} resulted in only less than 6% changes in $k_{21,0}$. For the autocatalytic reaction, we retained Smith et al.'s former rate coefficient expression,[31] $k_{35} = 1.32 \times 10^{12} \exp(-3070\ K/T)$ cm^3 mol^{-1} s^{-1}, because this expression was obtained simultaneously with that of

$k_{21,0}/[M] = 4.4 \times 10^{14} \exp(3163\ K/T)\ cm^6\ mol^{-2}\ s^{-1}$ from the molecular beam-mass spectrometric measurements of SO_3 formation rate in their SO_2 doped $CO/O_2/Ar$ flames. Later, in the computer simulation of species profiles for the same flames above, these authors reduced the A-factor of their k_{35} by a factor of 3 by employing Troe's $k_{21,0}/[M]$, instead of their previously determined values. Again we observed less than 6% changes in $k_{21,0}$ when we used the latter k_{35} expression of Smith et al. Overall, in our experimental conditions, the uncertainties in $k_{21,0}$ values due to the coupling of R21 with other SO_2 reactions are small, and are within the scatter of the experimental data.

The τ_{max} values from SO_2 rich mixtures at low temperatures are large. For example, $\tau_{max} = 2.6$ ms for a 3% SO_2/ 0.5% H_2/ 10.0% O_2/86.5% Ar mixture at $T = 1040$ K and $P = 1.47$ atm. Whether our data were contaminated by the flow disturbance(s) (contact surface and/or rarefaction wave) is next discussed: The determined $k_{21,0}$ values from experiments of widely different τ_{max} values agreed with one another within the scatter of the data (see Figure 7). Furthermore, some of the experiments performed with a very long time span showed the appearance of the second OH absorption peak (or hump) a long time after the first one. This is evidence of flow disturbance by the interaction of the reflected shock with either the contact surface or the rarefaction wave. Simple calculations for the locations of the contact surface and the rarefaction wave at the condition given above show that the time for the contact surface to meet the reflected shock was 2.8 ms and that the rarefaction wave did not cross the contact surface at all. Thus we concluded that our data were not contaminated by later stage flow disturbance(s).

Taking into account all of the uncertainties discussed above plus additional uncertainties for mixture composition, P_0, shock speed, signal-to-noise ratio, etc., we estimated maximum uncertainty limits, $U = \pm (\Sigma U_i^2)^{1/2} = \pm 2.5$ for the individual runs.

Figure 8 displays all of the existing experimental data for $k_{21,0}$/[M] together with the RRK calculation by Troe.[32] A non-Arrhenius fit to the data is given by

$$k_{21.0}/[\mathrm{M}] = 1.3 \times 10^{24}\, T^{-2.5} \exp(-2350\ \mathrm{K}/T)\ \mathrm{cm^6\ mol^{-2}\ s^{-1}}$$

for $T = 300$ - 2500 K with uncertainty limits of ±2.5. Because of the limitation imposed on the rate coefficient expression (non-Arrhenius), it is difficult to delineate satisfactorily both low and high temperature data. As seen in the figure, this expression represents the low temperature results quite well but at high temperatures it completely misses the results of Astholz et al. However, there is reasonable agreement with the data of Smith et al., especially if we consider the curved nature of their activation energy – lower at low temperatures, $T < 1500$ K and *vice versa* at high temperatures, $T > 1800$ K (see Figure 6).

The rate coefficients from our expression are compared with those of previous studies. At $T = 1050$ K, our rate coefficient (3.9×10^{15} cm^6 mol^{-2} s^{-1}) is about a factor of 6 smaller than that of Astholz et al.[28] (2.2×10^{16} cm^6 mol^{-2} s^{-1}), and a factor of 2 smaller than that of Smith et al.[31] (9.0×10^{15} cm^6 mol^{-2} s^{-1}). It is also about 40% larger than the theoretical value of Troe[32] (2.7×10^{15} cm^6 mol^{-2} s^{-1}). The occurrence of the peak value from our expression (4.0×10^{15} cm^6 mol^{-2} s^{-1}) is at 940 K while that from Troe's expression is at 660 K. Recently, Mueller et al.[44] reported a high pressure limit rate coefficient expression, $k_{21,\infty} = 9.20 \times 10^{10} \exp(-1198\ \mathrm{K}/T)$ cm^3 mol^{-1} s^{-1}. This expression

was derived using their measured rate coefficients at $T = 950$ - 1040 K and at $P = 0.5$ - 10.0 atm, the low pressure limit $k_{21,0}$/[M] expression of Troe and the Lindemann-Hishelwood interpolation formula. Unfortunately, a direct comparison could not be made between the results of this study and Mueller et al. because of the different experimental conditions employed. Thus we compare our $k_{21,0}$ values with $k_{21,eff}$ of Mueller et al. both computed at our experimental conditions (Figure 6). In the temperature range of this study, our $k_{21,0}$ values are greater than $k_{21,eff}$ of Mueller et al. by a factor of 4.

Finally, reaction flux analyses show that SO_3 is produced mainly by R21 ($SO_2 + O + M \rightarrow SO_3 + M$) and consumed by R –32 ($SO_2 + OH \leftarrow SO_3 + H$) throughout the reaction time. At τ_{max}, SO_3 is also consumed with a lesser extent (ca. 10 - 20%) by R –40 ($HOSO_2 + O_2 \leftarrow SO_3 + HO_2$). SO_3 production through R30 ($SO_2 + OH + M \rightarrow HOSO_2$) followed by R40 ($HOSO_2 + O_2 \rightarrow SO_3 + HO_2$) shows some flux only at early times of reaction. With our rate coefficients of R21, the observed conversion of S(IV) (SO_2) to S(VI) ($SO_3 + HOSO_2 + H_2SO_4$) was about 2%.

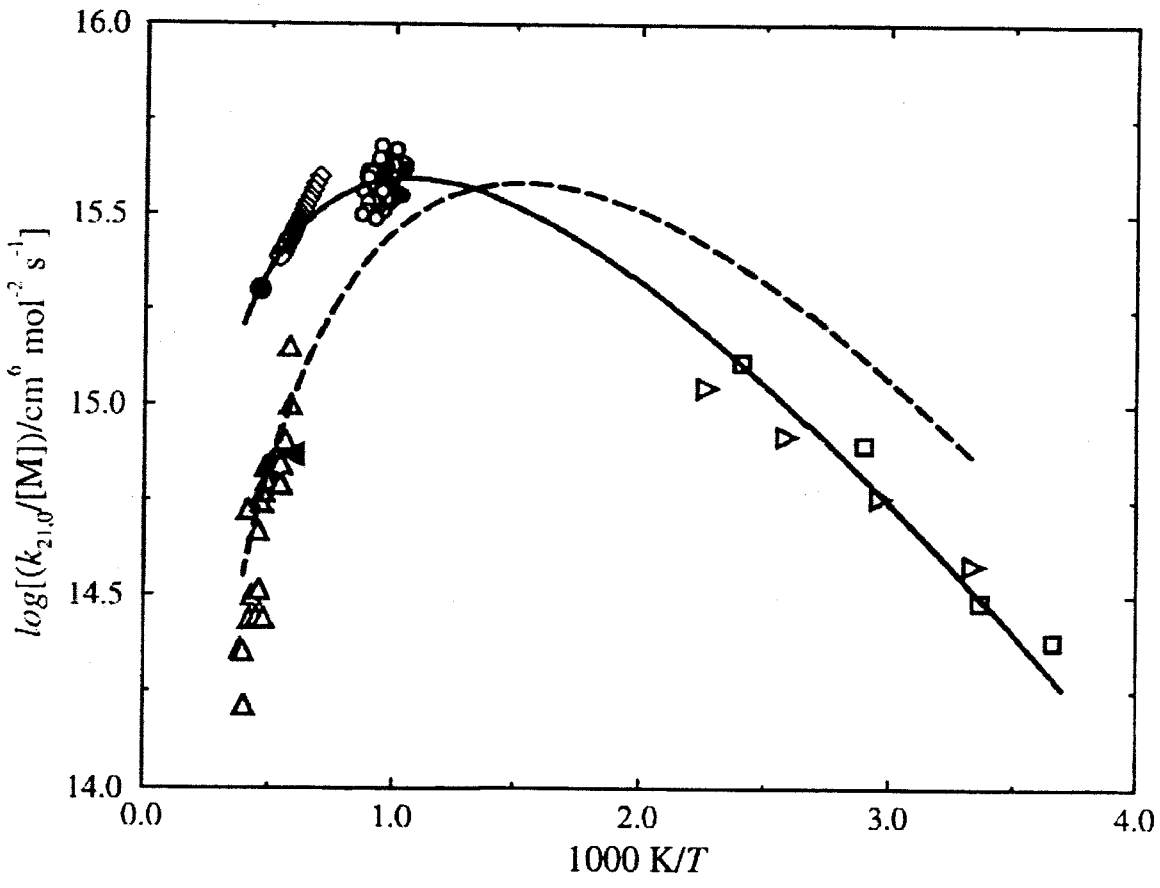

Figure 8: Low pressure limit rate coefficient data of R21. Symbols are: ●, Nettleton and Stirling;[26] □, Westenberg and deHaas;[27] △, Astholz et al.;[28] ▷, Atkinson and Pitts; [29] ◀, Merryman and Levy; [30] ◊, Smith et al.;[31] ○, this study. Lines are non-Arrhenius fits to the data: – –, Troe,[32] $k_{21,0}/[M] = 4.0 \times 10^{28}\ T^{-4.0} \exp(-2640\ K/T)$ cm^6 mol^{-2} s^{-1}; –, this study, $k_{21,0}/[M] = 1.3 \times 10^{24}\ T^{-2.5} \exp(-2350\ K/T)$ cm^6 mol^{-2} s^{-1} over T = 300 - 2500 K.

Conclusions

Thermochemical and structural data for HS, HSO, HOSO, HSO_2, and $HOSO_2$ were critically reviewed and thermodynamic data for these species were calculated (Appendix B).

A comprehensive but truncated reaction mechanism for the $SO_2/H_2/O_2$ system with the best available rate coefficients was assembled (Table II). Optimum $SO_2/H_2/O_2/Ar$ mixture compositions and experimental conditions were established via a series of sensitivity analyses. Shock tube experiments were performed using an OH laser absorption spectroscopic technique. The measured absorption coefficients of SO_2 at $\lambda = 310.032$ nm in air is

$$\sigma_{SO2} = 1.3 \times 10^5 \exp(-180\ \mathrm{K}/T)\ \mathrm{cm}^2\ \mathrm{mol}^{-1}$$

The experimental results were analyzed via computer simulations. In our experimental conditions, the title reaction is in low pressure limits. The rate coefficient expression is

$$k_{21,0}/[\mathrm{M}] = 3.9 \times 10^{15}\ \mathrm{cm}^6\ \mathrm{mol}^{-2}\ \mathrm{sec}^{-1}$$

over the temperature and density range of $T = 960$ - 1150 K and $\rho = 16$ - 30 μmol cm^{-3} ($P =$ 1.25 - 2.65 atm), respectively, with uncertainty limits of ±2.5. A non-Arrhenius fit to our data together with all existing data gives

$$k_{21,0}/[\mathrm{M}] = 1.3 \times 10^{24}\, T^{-2.5} \exp(-2350\ \mathrm{K}/T)\ \mathrm{cm}^6\ \mathrm{mol}^{-2}\ \mathrm{s}^{-1},$$

at $T = 300$ - 2500 K with the same uncertainty limits. The observed conversion of S(IV) (SO_2) to S(VI) ($SO_3 + H_2SO_4$) was about 2%.

References

1. Minnus, P.; Young, D. F.; Garber, D. P. *Geophys. Res. Lett.* **1998**, *25,* 1157.
2. Changnon, S. A. *J. Appl. Meteorol.* **1981**, *20*, 496.
3. Sassen, K. *Bull. Am. Meteorol. Soc.* **1997**, *78*, 1885.
4. Duda, D. P.; Minnis, P.; Nguyen, L. *J. Geophys. Res.* **2001**, *106*, 4927.
5. Meerkotter, R. *Ann. Geophys.* **1999**, *17*, 1080.
6. Travis, D. J.; Carleton, A. M; Lauritsen, R. G. *Nature* 2002, *418*, 601.
7. Arnold, F.; Scheid, J.; Stilp, T.; Schlager, H.; Reinhardt, M. E. *Geophys. Res. Lett.* **1992**, *19*, 241.
8. Fahey, D. W. *J Geophys. Res.* **1995**, *100*, 3065.
9. Busen, R.; Schumann, U. *Geophys. Res. Lett.* **1995**, *22*, 1357.
10. Hoffmann, D. J.; Rosen, J. M. *Geophys. Res. Lett.* **1978**, *5*, 511.
11. Zhao, J.; Turco, R. P. *J. Aerosol Sci.* **1995**, *26*, 779.
12. Kärcher B.; Peter, T.; Ottmann, R. *Geophys. Res. Lett.* **1995**, *22*, 1501.
13. Fahey, D. W.; Keim, E.R. *Science* **1995**, 270.
14. Danilin, M. Y.; Rodriguez, J. M.; Ko, M. K. W.; Weisenstein, D. K.; Brown, R. C.; Miake-Lye, R. C.; Anderson, M. R. *J. Geophys. Res.* **1997**, *102*, 21453.
15. Kärcher, B.; Fahey, D. W. *Geophys. Res. Lett.* **1997**, *24*, 389.
16. Yu, F.; Turco, R. P. *J. Geophys. Res.* 1998, *103*, 25915.

17. Curtius, J.; Sierau, B.; Arnold, F.; Baumann, R.; Busen, R.; Schulte, P.; Schumann, U. *Geophys. Res. Lett.* **1998**, *25*, 923.

18. Brown, R. C.; Miake-Lye, R.C.; Anderson, M. R.; Kolb, C. E. *Geophys. Res. Lett.* **1996**, *101*, 22939.

19. Arnold, F.; Stilp, T.; Busen, R.; Shumann, U. *Atmos. Environ.* **1998**, *32*, 3073.

20. Frenzel, A.; Arnold, F. *DLR-Mitt. 94* – 06, Dtsch. Zentrum für Luft- und Raumfahrt, Cologne, Germany, **1994**, 106.

21. Curtius, J.; Arnold, F.; Schulte, P. *Geophys. Res. Lett.* **2002**, *29,* 7.

22. Schroder, F.; Brock, C. A.; Baumann, R.; Petzold, A.; Busen, R.; Schulte, P.; Fiebig, M. *J. Geophys. Res.* **2000**, *105*, 19,941.

23. Schumann, U.; Arnold, F.; Busen, R.; Curtius, J.; Karcher, B.; Kiendler, A.; Petzold, A.; Schlager, H.; Schroder, F.; Wohlfrom, K.-H. *J. Geophys. Res.* **2002**, *107*, NO. D15.

24. Schumann, U. *J Geophys. Res.* **1996**, *101*, 6853.

25. Schumann, U.; Schlager, H.; Arnold, F.; Ovarlez, J.; Kelder, H.; Hov, Ø.; Hayman, G.; Isaksen, I. S. A.; Staehelin, J.;Whitefield, P. D. *J. Geophys. Res.* **2000**, *105*, 3605.

26. Nettleton, M. A.; Stirling, R. *Twelfth Symp. (Int.) on Comb.* **1969**, 635.

27. Westenberg, A. A.; deHaas, N. *J. Chem. Phys.* **1975**, *63*, 5411.

28. Astholz, D. C.; Glanzer, K.; Troe, J. *Eleventh Symp. (Int.) on Comb.* **1977**, 232.

29. Atkinson, R.; Pitts, J. N. *Int. J. Chem. Kinet.* **1978**, 1081.

30. Merryman, E. L.; Levy, A. *Seventeenth Symp. (Int.) on Comb.* **1978**, 727.

31. Smith, O. I.; Tseregounis, S.; Wang, S. *Int. J. Chem. Kinet.* **1982**, *14*, 679 - 697.

32. Troe, J. *Ann. Rev. Phys. Chem.* **1978**, *29*, 233.

33. Gardiner, W. C., Jr.; Walker, B. B.; Wakefield, C. B. In *Shock Waves in Chemistry*; Lifshitz, A., Ed.; Marcel Dekker: New York **1981**; Chapter 7.

34. McBride, B. J.; Michael, J. Z.; Gordon, S. *NASA Glenn Coefficients for Calculating Thermodynamic Properties of Individual Species*; NASA TP-211556; Cleveland, Ohio, 2002.

35. Hwang, S. M.; Ryu, Si-OK; De Witt, K. J. ; Rabinowitz, M. J. *J. Phys. Chem. A* **1995**, *103*, 5949.

36. Michael, J. V.; Sutherland, J. W. *Int. J. Chem. Kinet.* **1986**, *18*, 409.

37. Hwang, S. M.; Ryu, Si-OK; De Witt, K. J.; Rabinowitz, M. J. "*Rate Coefficient Determination fo H + O2 → productes,"* paper in preparation, 2003 and references there in.

38. Ruscic, B.; Wagner, A. F.; Harding, L. B.; Asher, R. L.; Feller, D.; Dixon, D. A.; Peterson, K. A.; Song, Y.; Qian, X.; Ng, C.-Y.; Liu, J.; Chen, W.; Schwenke, D. W. *J. Phys. Chem. A* **2002**, *106*, 2727.

39. Gurvich, L. V.; Veyts, I. V.; Alcock, C. B. "Thermodynamic Properties of Individual Substances." Vol. 1, parts 1 and 2; Hemisphere Publishing Corp.: New York, 1989.

40. Chase, M. W., Jr.; Davis, C. A.; Downey, J. R.; Frurip, D. J.; McDonald, R. A.; Syverud, A. N. *J. Phys. Chem. Ref. Data* **1985**, *14*, Suppl. 1.

41. Radhakrishnan, K.; Hindmarsh, A. C. *Description and Use of LSODE, The Livermore Solver for Ordinary Differential Equations;* NASA RP 1327; Washington, D.C., 1993.

42. Kee, R. J.; Rupley, G. M.; Miller, J. A. *Chemkin-II: A Fortran Chemical Kinetics Package for the Analysis of Gas-Phase Chemical Kinetics;* Report SAND89-8009; Sandia National Laboratories: Livermore, CA, 1989.

43. Radhakrishnan, K. *LSENS- A General Chemical Sensitivity and Analysis Code for Homogeneous Gas-Phase Reactions;* NASA RP 1328; National Aeronautics and Space Administration: Washington, DC, 1994.

44. Vandaele, A. C.; Simon, P. C. *J. Geophy. Res.* **1994**, *99*, 25599.

45. Mueller, M. A.; Yetter, R. A.; Dryer, F. L. *Int. J. Chem. Kinet.* **2000**, *32*, 317.

46. Atkinson, R.; Baulch, D. L.; Cox, R. A.; Hampson, R. F., Jr.; Kerr, J. A.; Rossi, M. J.; Troe, J. *J. Phys. Chem. Ref. Data* **1997**, *26*, No. 6, 1454.

47. Carleton, K. L.; Kessler, W. J.; Marinelli, W. *J. Phys. Chem.* **1993**, *97*, 6412.

48. Gutman, D.; Hardwidge, E. A.; Dougherty, F. A.; Lutz, R. W. *J. Chem. Phys.* **1967**, *47*, 5950.

49. Baulch, D. L.; Cobos, C. J.; Cox, R. A.; Frank, P.; Hayman, G.; Just, Th.; Kerr, J. A.; Murrells, T.; Pilling, M. J.; Troe, J.; Walker, R. W.; Warnatz, J. *J. Phys. Chem. Ref. Data* **1994**, *23*, 847.

50. Kallend, A. S. *Combust. Flame* **1972**, *19*, 227.

51. Binns, D.; Marshall, P. *J. Chem. Phys.* **1991**, *95*, 4940.

52. Goumri, A.; Rocha, J.-D.; Laakso, D.; Smith, C. E.; Marshall, P. *J. Phys. Chem. A* **1999**, *103*, 11328.

53. Chiang, H.-M. Ph.D. Thesis, Department of Chemical Engineering, Chemistry, and Environmental Science, New Jersey Institute of Technology, Newark, NJ, 1995.

54. Schumann, U.; Arnold, F.; Busen, R.; Curtius, J.; Karcher, B.; Kiendler, A.; Petzold, A.; Schlager, H.; Schroder, F.; Wohlfrom, K.-H. *J. Geoph. Res.* **2002**, *107*, No. D15.

55. Kieffer, J. H.; Ramaprabhu, R. *Chem. Phys. Lett.* **1982**, *86*, 499.

56. Lovejoy, E. R.; Hanson, D. R.; Huey, G. L. *J. Phys. Chem.* **1996**, *100*, 19911.

Appendix A

Computer Modeling/Simulation

The general purpose of computer modeling is to simulate the experimental results. Once a match between the experimental and the predicted data is achieved the model parameters are regarded as the best estimates. The foundation for this computer modeling is solving a set of coupled first-order ordinary differential equations for species simultaneously.[23] Figure 1A shows the schematic of the computer model. The goal of the computer modeling employed in this study is to obtain reaction rate coefficients for specific chemical reactions by matching the experimental observables with the model prediction.

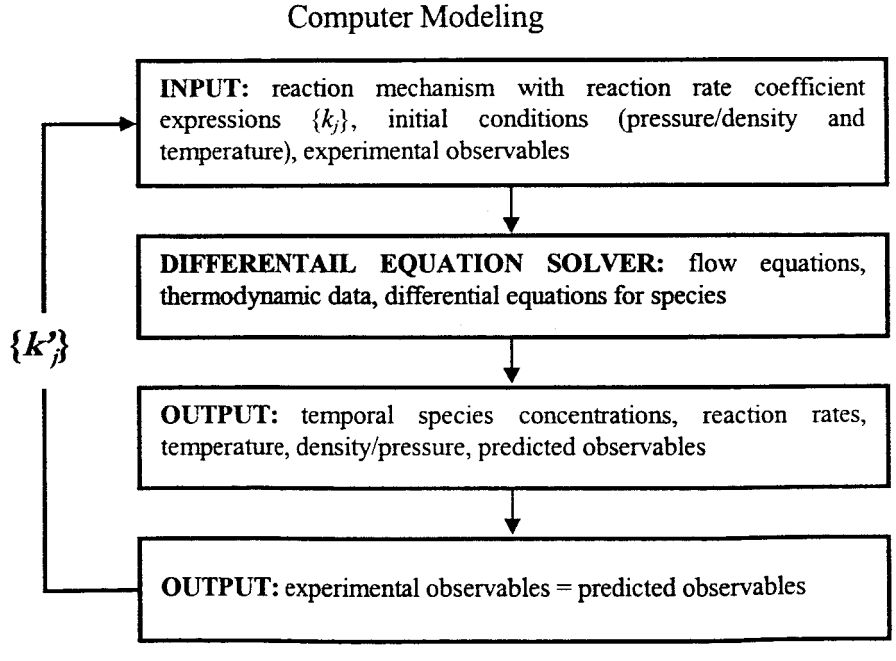

Figure 1A: Block Diagram for Computer Simulation

Reaction Rates

All chemical reactions may be assumed to be reversible. For an irreversible reaction the reverse rate coefficient would be extremely small or zero. Here the forward rate coefficient of reaction will be referred to as k_f and the reverse will be referred to as k_r. Usually the input for the computer model (reaction mechanism) provides for k_f. k_r is calculated using the equilibrium constant, K_c. K_c is calculated using thermodynamic data. As an example, for a reaction:

$$aA + bB = cC + dD \qquad \text{(A-1)}$$

The Gibbs free energy change is:[24]

$$\Delta G = \Delta H - T\,\Delta S \qquad \text{(A-2)}$$

Here ΔG is calculated from ΔH and ΔS using thermodynamic data for species A, B, C, and D at a given temperature T. The relationship between the Gibbs free energy and the equilibrium constant of a reaction is[24]

$$K_p = \exp(-\Delta G/RT). \qquad \text{(A-3)}$$

K_c is related to K_p using the relationship of equilibrium constants in terms of pressure and concentration:

$$K_c = K_p(RT)^{-\Delta n} \qquad \text{(A-4)}$$

where $\Delta n = (c + d) - (a + b)$.

Then the microscopic reversibility for (A-1) gives:

$$k_r = k_f / K_c \qquad \text{(A-5)}$$

As chemical reactions proceed the concentrations of each species change as they are either consumed or produced. When the concentrations change, system temperature and density/pressure also change. Therefore, all values for each of the derivatives must be re-evaluated for each time step.

The first step in modeling is to develop an initial reaction mechanism. A reaction mechanism is a set of chemical reactions with corresponding rate coefficient expressions that have the ability to predict the actual chemical reaction systems. In order to simulate the behavior of a system accurately the reaction mechanism must be comprehensive. Each reaction within the reaction mechanism has its own specific reaction rate. The modeling process becomes simpler if many of these rates are known from prior experimentation/calculations. Some rates would have to be assumed. Optimizing a target reaction rate is an inverse problem. For this purpose, experimental conditions must be selected such that the target reaction has the dominant sensitivity on experimental observables. Usually this is done using a sensitivity analysis as described below.

Sensitivity Analysis

The local logarithmic sensitivity, defined below[25], is use throughout this study.

$$S_{ij} = \frac{\ln\left(\frac{Q_i'}{Q_i}\right)}{\ln\left(\frac{k_j'}{k_j}\right)} \qquad \text{(A-6)}$$

Here k_j is a rate coefficient of reaction j and Q_i is the response of observable i. The prime (') symbol indicates the value after a change has occurred. In a sensitivity analysis a reaction rate coefficient is varied and the effect of this change on the observable is examined. If no change occurs in the observable then that reaction is said to have no sensitivity. If a change in the reaction rate coefficient causes the response to change then the reaction is said to be sensitive.

Appendix B

Hydroxysulfonyl ($HOSO_2$)

$\Delta_f H^0_{298.15} = -93.5$ *k*cal mol^{-1}

Vibrational Frequencies (cm^{-1}) and Degeneracies:
3539.8 (1)
1309.2 (1)
1296.2 (1)
1097.2 (1)
759.3 (1)
544 (1)
491 (1)
437 (1)
252 (1) – torsion

Ground State Quantum Weight: 2 (^{2}A')

Point Group: C_1

External Rotational Symmetry Number: $\sigma = 1$

Bond Length (angstrom):
r(S-O1) = 1.612
r(S-O2) = 1.444
r(S-O3) = 1.436
r(O1-H) = 0.967

Bond Angle (degree):
θ(S-O1-H) = 107.2
θ(O1-S-O2) = 108.4
θ(O1-S-O3) = 106.0

τ(O2-S-O1-H) = 26.1
τ(O3-S-O1-H) = 161.1

Product of the Moment of Inertia: $I_xI_yI_z = 1.473 \times 10^{-114}$ g^3 cm^6
Reduced Moment of Inertia: $I_r = 1.405 \times 10^{-40}$ g cm^2
Internal Rotational Symmetry Number: n = 2
Barrier to Internal Rotation: $V_0 = 2.271$ *k*cal mol^{-1}

Enthalpy of Formation

From Benson's estimate[1] for $D^0_{298.15}$(HO-SO$_2$) = 36 ± 3 kcal mol^{-1}, $\Delta_fH^0_{298.15}$ = –98 *k*cal mol^{-1} (–409 *k*J mol^{-1}) was derived. This value of $\Delta_fH^0_{298.15}$ gives $\Delta_rH^0_{298.15}$ = 6 *k*cal mol^{-1} for the reaction, $HOSO_2 + O_2 \rightarrow HO_2 + SO_3$.

Margitan's rate coefficients measurement[2] for the above reaction put an upper limit for the reaction endothermicity, $\Delta_rH^0_{298.15} \leq 2$ *k*cal mol^{-1} ($D^0_{298.15}$(HO-SO$_2$) ≤ 32 *k*cal mol^{-1}). Gleason and Howard[3] set a limit on the endothermicity of the reaction (1), $\Delta_rH^0_{298.15} \leq 3$ *k*cal mol^{-1}, which places a lower limit of $\Delta_fH^0_{298.15} \geq$–94.5 *k*cal mol^{-1} ($\geq$–395.4 *k*J mol^{-1}). Here we adopted Margitan's value of $\Delta_rH^0_{298.15}$ = 2 *k*cal mol^{-1}, which gives $\Delta_rH^0_{298.15}$ = –93.5 *k*cal mol^{-1} (–391.2 *k*J mol^{-1}).

Heat Capacity and Entropy

The molecular structure of $HOSO_2$ was taken from the results of MP2 level calculation with cc-pVQZ basis set by Majumdar er al.[4] The reduced moment of inertia, I_r, for the hindered internal rotation was calculated by assuming $HOSO_2$ is essentially a *cis* form.[4]

This assumption sets the internal rotational symmetry number, n = 2. The rotational barrier was calculated using the equation, $2\pi c\omega/n = (V_0/2I_r)^{1/2}$, where c is the speed of light and ω is the torsional frequency, 252 cm^{-1}.

Hashimoto et al.[5] measured four vibrational frequencies of $HOSO_2$ in an argon matrix at 11 K. Nagase et al.[6] confirmed the four vibrational frequencies using the same method of Hashimoto et al. and also calculated the geometry and vibrational frequencies at the unrestricted HF level with the 3-21G(*) bases set. Later, Kuo et al.[7] measured vibrational frequencies of $HOSO_2$ in the argon matrix at 12 K. The four frequencies reported by Hashimoto et al. and Nagase et al. were again confirmed. An additional frequency corresponding to HOS bend at 1296.2 cm^{-1} was measured.[7] Here, we took five experimental frequencies (3539.8, 1309.2, 1296.2, 1097.2, 759.3) of Hashimoto et al., Nagase et al. and Kuo et al. and four computed frequencies (544, 491, 437, 252) of Nagase et al. for the derivation of heat capacity and entropy.

Hydroxysulfinyl (HOSO)

$\Delta_f H^0(0\ K) = -56.7 \pm 2.4$ *k*cal mol^{-1}

Vibrational Frequencies (cm^{-1}) and Degeneracies:
3476 (1)
1351 (1)
1073 (1)
764 (1)
343 (1)
200 (1) – torsion

Ground State Quantum Weight: 2 (^{2}A")

Point Group: C_s

External Rotational Symmetry Number: $\sigma = 1$

Bond Length (angstrom):
r(S-O1) = 1.661
r(S-O2) = 1.482
r(O1-H) = 0.983

Bond Angle (degree):
θ(S-O1-H) = 106.9
θ(O1-S-O2) = 109.8

Product of the Moment of Inertia: $I_xI_yI_z = 2.539 \times 10^{-115}$ g^3 cm^6

Reduced Moment of Inertia: $I_r = 1.585 \times 10^{-40}$ g cm^2

Internal Rotational Symmetry Number: n = 2

Barrier to Internal Rotation: $V_0 = 1.888$ *k*cal mol^{-1}

Enthalpy of Formation, Heat Capacity and Entropy

The enthalpy of formation of HOSO and its geometry and vibratoinal frequencies have not been measured experimentally. The most reliable information is from theoretical calculations of Laakso et al.[8] Laakso et al. optimized geometry and vibrational frequencies at the MP2=FULL/6-31G* level. Energies were obtained with G2 theory. For the enthalpy of formation, the changes in G2 energy for the reaction, HOSO → OH + SO ($\Delta_rH^0_0 = -67.11$ *k*cal mol^{-1}) were obtained and then $\Delta_fH^0_0$ of HOSO was derived using the measured $\Delta_fH^0_0$ values of OH and SO in the JANAF tables.[9] Laakso et al. proved the reliability of their calculation by comparing their G2 level $\Delta_rH^0_0$ for the reaction, HS + O_2 → OH + SO, with that of the experimental value from the JANAF tables. Only a small difference in the reaction enthalpy, Δ_rH^0(0 K) = 0.0717 *k*cal mol^{-1}, resulted.

However, a recent measurement and quantum calculation of D^0_0(OH) = 8.85 ± 0.07 *k*cal mol^{-1} (37.03 ± 0.29 *k*J mol^{-1}). Thus the calculated $\Delta_f H^0_0$ value for HS + O_2 → OH + SO reaction by Laakso et al. would be different from 0.0717 *k*cal mol^{-1}. Since D^0_0 for HOSO dissociation from Laakso et al. is the only available value, we adopted this value and calculated the enthalpy of formation of HOSO using the newly measured $\Delta_f H^0$ of OH and the NASA value of SO at 0 K. The recommended enthalpy of formation of HOSO is $\Delta_f H^0$(HOSO, 0 K) = $\Delta_f H^0_0$(OH) + $\Delta_f H^0_0$(SO) – 66.729 = 8.85 + 1.1267 – 66.729 *k*cal mol^{-1} = –56.7 ± 2.4 *k*cal mol^{-1} (–237.4 ± 10 *k*J mol^{-1}) with an error bound given by Laakso et al.

For the derivation of heat capacity and entropy we took the molecular geometry and vibrational frequencies of Laakso et al. The barrier to internal rotation (V_0 = 1.888 *k*cal mol^{-1}) was directly taken from Laakso et al.'s computed G2 barrier for *cis* to *trans* transition of HOSO.

Sulfinyl (HSO_2)

$\Delta_f H^0_{298.15}$ = –42.580 ± 2.008 *k*cal mol^{-1}

Vibrational Frequencies (cm^{-1}) and Degeneracies:
2269 (1)
1600 (1)
1128 (1)
1065 (1)
810 (1)
431 (1) – torsion

Ground State Quantum Weight: 2 (^{2}A')

Point Group: C_s

External Rotational Symmetry Number: $\sigma = 1$

Bond Length (angstrom):
r(S-O1) = 1.447
r(S-O2) = 1.447
r(H-O2) = 1.381

Bond Angle (degree):
θ(O1-S-O2) = 123.2
θ(H-S-O2) = 105.6
τ(H-S-O2(O1)) = 121.1

Product of the Moment of Inertia: $I_xI_yI_z = 1.485 \times 10^{-115}$ g^3 cm^6

Enthalpy of Formation

Benson's[1] estimate for the enthalpy of formation of HSO_2 was $\Delta_fH^0_{298.15} = -42.580 \pm 2.008$ *k*cal mol^{-1} (-177.4 ± 16.7 *k*J mol^{-1}). The corresponding $D^0_{298.15}$ (H-SO_2) = 41 *k*cal mol^{-1} was compatible with the fast rate coefficients measured in flame studies at T > 1600 K for the three-body recombination reaction (H + SO_2 + M = HSO_2 + M). Boyd et al.[10] performed ab initio calculations for HSO_2 at the HF/STO-3G* level. Using the calculated $D^0_{298.15}$ (H-SO_2) = 33.9619 *k*cal mol^{-1} and the $\Delta_fH^0_0$ values of H and SO_2 in the JANAF tables,[9] $\Delta_fH^0_0 = -52.7$ *k*cal mol^{-1} (-220.4 *k*J mol^{-1}) was derived for HSO_2. Laakso et al.[8] optimized geometry and vibrational frequencies for HSO_2 at the MP2=FULL/6-31G* level. Energies were obtained with G2 theory. For the enthalpy of formation, the change in G2 energy for the reaction, $HSO_2 \rightarrow$ H + SO_2 ($\Delta_rH^0_0 = -13.575 \pm 2.39$ *k*cal mol^{-1}) was obtained and then $\Delta_fH^0_0$ of HSO_2 was derived using the measured $\Delta_fH^0_0$ values of H and SO_2 in the JANAF tables. $\Delta_fH^0_{298.15}$ of $HSO_2 = -33.8 \pm 2.4$ *k*cal mol^{-1} (-141.4 ± 10 *k*J

mol^{-1}) was recommended. Laakso et al. proved the reliability of their calculation by comparing their G2 level $\Delta_r H^0_0$ for the reaction, $HS + O_2 \rightarrow H + SO_2$ with that of the experimental value from the JANAF tables. Considering the error limit in the G2 $\Delta_r H^0_0$ value, the difference in the reaction enthalpy, $\Delta_r H^0_0 = -2.246$ *k*cal mol^{-1} was considered excellent. Recently, Dein and Ventura[11] investigated the enthalpy of formation of XSO_2, X = H, CH_3, using the B3LYP and B3PW91 methods with very large basis sets up to cc-pV6Z. The enthalpy of formation of HSO_2 is $\Delta_f H^0_{298.15} = -42.590 \pm 2.008$ *k*J mol^{-1}.

Heat Capacity and Entropy

Vibrational frequencies of HSO_2 have not been measured experimentally and only one theoretical calculation is available. For the derivation of heat capacity and entropy we used the vibrational frequencies calculated at the MP2=FULL/6-31G* level by Laakso et al.[8] The molecular geometry was taken from the theoretical calculation using the B3PW91 method with the cc-pV6Z basis set by Denis and Ventura.[11]

Mercapto (HS)

$\Delta_f H^0(0\ K) = -31.794$ *k*cal mol^{-1}

Enthalpy of Formation

The current JANAF[9] recommendations for $\Delta_f H^0_0 = -32.621 \pm 1.195$ *k*cal mol^{-1} and $\Delta_f H^0_{298.15} = -32.583 \pm 1.195$ *k*cal mol^{-1} are based on the measurements of HS ionization

potential and the appearance potential of HS^+ from photoionization of H_2S. The previous NASA recommendation[12] for $\Delta_f H^0_{298.15}$ was also 33.300 *k*cal mol^{-1}. Continetti and Lee[3] performed photodissociatoin of H_2S at 193.3 nm using H-atom photofragment-translational spectroscopy with mass spectroscopic detection. They found D^0(H-S) = 83.48 ± 0.69 *k*cal mol^{-1} (349.27 ± 2.89 *k*J mol^{-1}) in the secondary photodisociation of HS radicals, formed in the primary H_2S photodissociatoin experiments. Nicovitch et al.[14] measured the forward and reverse reaction rate coefficients of Br($^2P_{3/2}$) + H_2S = HS + HBr over the temperature range of 319 – 431 K. Using both the "second law method" and the "third law method", an average value of $\Delta_r H^0$ at a given temperature was obtained; then the values of $\Delta_r H^0_0$ and $\Delta_f H^0_{298.15}$ were calculated by applying heat capacity corrections from data in the JANAF tables for Br, H_2S, HS and HBr. The reported values for the enthalpy of formation and the bond dissociation energy are $\Delta_f H^0_0$ = –34.07 ± 0.72 *k*cal mol^{-1} (–142.55 ± 3.01 *k*J mol^{-1}), $\Delta_f H^0_{298.15}$ = 34.18 ± 0.68 *k*cal mol^{-1} (143.01 ± 2.85 *k*J mol^{-1}) and D^0_0(H-S) = [1]83.23 ± 0.78 *k*cal mol^{-1} (348.23 ± 3.26 *k*J mol^{-1}), $D^0_{298.15}$(H-S) = 84.12 ± 0.74 *k*cal mol^{-1} (351.96 ± 3.10 *k*J mol^{-1}), respectively. We adopted the bond dissociation energy of Continetti and Lee, D^0_0(H-S) = 83.48 ± 0.69 *k*cal mol^{-1} (349.27 ± 2.89 *k*J mol^{-1}) and derived $\Delta_f H^0_0 = \Delta_f H^0_0$(S) + $\Delta_f H^0_0$(H) – 83.476 = 64.653 + 50.621 – 83.476 = 31.80 *k*cal mol^{-1} (133.03 *k*J mol^{-1}).

Hydrogen Sulfur Oxide (HSO)

$\Delta_f H^0_0$ = –1.6 ± 0.7 *k*cal mol^{-1}

Vibrational Frequencies (cm^{-1}) and Degeneracies:
2480 (1)
1164 (1)

1026 (1)

Ground State Quantum Weight: 2 (^{2}A")

Point Group: C_1

External Rotational Symmetry Number: $\sigma = 1$

Bond Length (angstrom):
r(S-O) = 1.494
r(S-H) = 1.389

Bond Angle (degree):
θ(H-S-O) = 106.6

Product of the Moment of Inertia: $I_xI_yI_z = 5.028 \times 10^{-117}$ g^3 cm^6

Enthalpy of Formation

Schurath et al.[15] measured the chemiluminescence spectrum of the $X^2A'' \leftarrow A^2A'$ transition of HSO and DSO. The $\Delta_rH^0_{298.15}$ for the reaction HS + O_3 → HSO + O_2 (HS + O_3 → HSO* + O_2, HSO* → HSO) was estimated using the observed highest level of HS-O vibration, $v'_3 = 7$, which corresponds to 19149 cm^{-1} (54.74 *k*cal mol^{-1}). Using $-\Delta_rH^0_{298.15} \leq$ 54.74 *k*cal mol^{-1} and the values of the enthalpy of formation of HS and O_3 available, Schurath et al.[15] set an upper limit of $\Delta_fH^0_{298.15} \leq$14.9 *k*cal mol^{-1}. White and Gardiner[16] reanalyzed the results of Schurath et al. and presented $12.2 < \Delta_fH^0(298.15\ K) < 14.1$ *k*cal mol^{-1}. Benson's estimate[1] was $\Delta_fH^0_{298.15} = -5 \pm 4$ *k*cal mol^{-1}. Slagle et al.[17] suggested $\Delta_fH^0_{298.15} = -3$ *k*cal mol^{-1}, based upon their kinetic work on the reaction O(^{3}P) + H_2S → HSO + H. Davidson et al.[18] studied the reactive scattering of O atoms with H_2S molecules using a crossed molecular beam mass spectrometric detection of HSO radicals. The value of the enthalpy of formation obtained was $\Delta_fH^0_{298.15} = -1.4$ *k*cal mol^{-1} (-6 ± 8 *k*J mol^{-1}).

Balucani et al.[19] determined $\Delta_f H^0(0\ K) = -0.9 \pm 0.7$ *k*cal mol^{-1} (-3.8 ± 2.9 *k*J mol^{-1}) from the analysis of high resolution crossed beam reactive scattering experiments on the reaction $O(^3P) + H_2S \rightarrow HSO + H$. Here we took Balucani et al.'s $\Delta_f H^0(0\ K) = -0.9 \pm 0.7$ *k*cal mol^{-1} (-3.8 ± 2.9 *k*J mol^{-1}).

Heat Capacity and Entropy

The molecular geometries and vibrational frequencies of HSO and DSO radicals were determined by Schurath et al.,[15] Kakimoto et al.,[20] and Ohashi et al.[21] Following the measurements of Schurath et al., Kakimoto et al. and Ohashi et al. observed the Doppler-limited dye laser excitation spectra of the $A^2A'(003) \leftarrow X^2A''(000)$ vibronic transition of HSO and DSO. Here we took the structural parameters of HSO from those of Ohashi et al. and Kakimoto et al., instead of the "best fit" values used in vibronic band contour synthesis by Schurath et al. The product of moment of inertia, $I_xI_yI_z$, was calculated using the directly measured rotational constants B_x, B_y, and B_z of Ohashi et al.

The three ground state ($^2A''$) vibrational frequencies, H-SO stretching (ω_1), H-S-O bending (ω_2), and HS-O stretching (ω_3), were presented by Schurath et al.[15] From v'_3 progression, ω_3 (1013 cm^{-1}) was measured. ω_2 was estimated (1063 cm^{-1}) using the measured bending frequency of DSO and the isotope factor. For ω_1, the recommended –S-H group frequency (2570 cm^{-1}) by Herzberg et al.[22] was assigned. However, the harmonic force field analysis by Ohashi et al.[21] yielded $\omega_2 = 1164$ cm^{-1} and $\omega_3 = 1026$ cm^{-1}. The force constant, k_1, was estimated by applying Badger's rule using the bond lengths and force constants of HS($^2\Pi$)

and HS($^2\Sigma^+$) as references. From this estimated force constant $\omega_1 = 2271$ cm^{-1} was calculated.

Here we adopted $\omega_2 = 1164$ cm^{-1} and $\omega_3 = 1026$ cm^{-1} of Ohashi et al. We believe the ω_1 value from –S-H group frequency is too high and that of Ohashi et al. too low. Therefore we estimated the ω_1 value in the following manner: Using the known H-O and H-OO stretching frequencies the force constant change from H-O to H-OO was calculated. For H-OO stretching the force constant was reduced by 15% from that of H-O. Since HS and HSO are isovalent radicals of HO and HOO, respectively, we calculated the force constant of H-SO by applying the same 15% reduction to the H-S force constant. The ω_1 value was calculated to be $\omega_1 = (1/2\pi c)(k_1/m_H)^{1/2} = 2480$ cm^{-1}, where c is the speed of light and m_H is the mass of the terminal H atom.

References

1. Benson, S. W. *Chem. Rev.* **1978**, *78*, 23.
2. Margitan, J. J. *J. Phys. Chem.* **1984**, *88*, 3314.
3. Gleason, J. F.; Howard, C. J. *J. Phys. Chem.* **1988**, *92*, 3414.
4. Majumdar, D.; Kim, J.; Oh, K. S.; Lee, J. Y.; Choi, W. Y.; Lee, S.-H.; Kang, M.-H.; Min, B. J. *J. Chem. Phys.* **2000**, *112*, 723,
5. Hashimoto, S.; Inoue, G.; Akimoto, H. *Chem. Phys. Lett.* **1984**, *107*, 198.
6. Nagase, S.; Hashimoto, S.; Akimoto, H. *J. Phys. Chem.* **1988**, *92*, 641.
7. Kuo, Y.-P.; Cheng, B.-M.; Lee, Y.-P. *Chem. Phys. Lett.* **1991**, *177*, 195.
8. Laakso, D.; Smith, C. E.; Goumri, A.; Rocha, J.-D. R.; Marshal, P. *Chem. Phys. Lett.* **1994**, *227*, 377.

9. Chase, M. W., Jr.; Davis, C. A.; Downey, J. R.; Frurip, D. J.; McDonald, R. A.; Syverud, A. N. *J. Phys. Chem. Ref. Data* **1985**, *14*, Suppl. 1.

10. Boyd, R.; Gupta, A.; Langler, R. F.; Lownie, S. P.; Pincock, J. Can, *J. Chem.* **1980**, *58*, 331.

11. Denis, P. A.; Ventura, O. *Chem. Phys. Lett.* **2001**, *344*, 221.

12. McBride, B. J.; Michael, J. Z.; Gordon, S. *NASA Glenn Coefficients for Calculating Thermodynamic Properties of Individual Species*; NASA TP-211556; Cleveland, Ohio, 2002.

13. Continetti, R. E.; Balko, B. A.; Lee, Y. T. *Chem. Phys. Lett.* **1991**, 182, 400.

14. Nicovich, J. M.; Kreutter, K. D.; van Kijk, C. A.; Wine, P. H. *J. Phys. Chem.* **1992**, *96*, 2518.

15. Schurath, U.; Weber, M.; Bechker, K. H. *J. Chem. Phys.* **1977**, *67*, 110.

16. White, J. N.; Gardiner, W. C., Jr. *Chem. Phys. Lett.* **1978**, *58*, 470.

17. Slagle, I. R.; Baiocchi, F.; Gutman, D. *J. Phys. Chem.* **1978**, *82*, 1333.

18. Davidson, F. E.; Clemo, A. R.; Duncan, G. L.; Browett, R. J.; Hobson, J. H.; Grice, R. *Mol. Phys.* **1982**, *46*, 33.

19. Balucani, N.; Casavecchia, P.; Stanges, D.; Volpi, G. G. *Chem. Phys. Lett.* **1993**, *211*, 469.

20. Kakimoto, M.; Saito, S.; Hirota, E. *J. Mol. Spectrosc.* **1980**, *80*, 334.

21. Ohashi, N.; Saito, S.; Hirota, E. *J. Mol. Spectrosc.* **1980**, *84*, 204.

22. Herzberg, G. *Molecular Spectra and Molecular Structure II. Inrared and Raman Spectra of Polyatomic Molecules*; Van Nostrand: New York, **1945**.

23. Gardiner, W. C., Jr. In *Combustion Chemistry;* Gardiner, W. C., Jr. Ed.; Springer-Verlag: New York, **1984**; Chapter 1.

24. Atkins, P. W. *Physical Chemistry 2nd Ed.*; WH Freeman and Co.: San Francisco, 1982.

25. Gardiner, W. C., Jr. *J Phys. Chem.* **1979**, *83*, 37.